Island Arc

Island Arc (2012) **21**, 327–350

Research Article

Geochemistry and Sr–Nd–Pb isotopic constraints on the petrogenesis of Cenozoic lavas from the Pali Aike and Morro Chico area (52°S), southern Patagonia, South America

Mi Kyung Choo,[1,2] Mi Jung Lee,[1]* Jong Ik Lee,[1] Kyu Han Kim,[2] and Kye-Hun Park[3]

[1]*Division of Polar Earth System Sciences, Korea Polar Research Institute (KOPRI), Incheon 406-840, Korea (mjlee@kopri.re.kr),* [2]*Department of Sciences Education, Ewha Womans University, Seoul 120-750, Korea, and* [3]*Department of Earth Environmental Science, Pukyong National University, Busan 608-737, Korea*

Abstract Geochemical and isotopic analyses (Sr–Nd–Pb) of late Miocene to Quaternary plateau lavas from the Pali Aike and Morro Chico areas (52°S) were undertaken to constrain the melting processes and mantle sources that contributed to magma generation and the geodynamic evolution of southernmost Patagonia, South America. The Pali Aike and Morro Chico lavas are alkaline (Pali Aike, 45–49 wt.% SiO_2; 4.3–5.9 wt.% Na_2O+K_2O) and subalkaline (Morro Chico, 50.5–50.8 wt.% SiO_2; 4.0–4.4 wt.% Na_2O+K_2O), relatively primitive (Pali Aike, 9.5–13.7 wt.% MgO; Morro Chico, 7.6–8.8 wt.% MgO) mafic volcanic rocks that have typical intraplate ocean island basalt-like signatures. Incompatible trace element ratios and isotopic ratios of the Pali Aike and Morro Chico lavas differ from those of the majority of Neogene southern Patagonian slab window lavas in showing more enriched characteristics and are similar to high-μ (HIMU)-like basalts. The rare earth element (REE) modeling to constrain mantle melting percentages suggests that these lavas were produced by low degrees of partial melting (1.0–2.0% for Pali Aike lavas and about 2.6–2.7% for Morro Chico lavas) of a garnet lherzolite mantle source. The major systematic variations of Sr–Nd–Pb isotopes in southern Patagonian lavas are related to geographic location. The Pali Aike and Morro Chico lavas from the southernmost part of Patagonia have lower $^{87}Sr/^{86}Sr$ and higher $^{143}Nd/^{144}Nd$ and $^{206}Pb/^{204}Pb$ ratios, relative to most of the southern Patagonian lavas erupted north of 49.5°S, pointing to a HIMU-like signature. An isotopically depleted and HIMU-like asthenospheric domain may have been the main source of magmas in the southernmost part of Patagonia (e.g. Pali Aike, Morro Chico, and Camusu Aike volcanic field), suggesting the presence of a major discontinuity in the isotopic composition of the asthenosphere in southern Patagonia. On the basis of geochemical and isotope data and the available geological and geotectonic reconstructions, a link between the HIMU asthenospheric mantle domain beneath southernmost Patagonia and the HIMU mega-province of the southwestern Pacific Ocean is proposed.

Key words: Asthenosphere, HIMU-like ocean island basalt, Morro Chico, Pali Aike, Patagonia, Sr–Nd–Pb isotopes.

INTRODUCTION

The origin of alkali magmatism in continental extension zones has been the focus of many petrological studies that seek to determine the relative contributions of mantle plume material, convectively upwelling asthenospheric mantle, and thermally activated lithospheric mantle. Trace element and isotopic compositions of these magmas can provide information regarding both the nature of mantle sources and the tectonic history of extensional areas.

*Correspondence.

Received 21 November 2011; accepted for publication 2 September 2012.

doi:10.1111/iar.12002

In Patagonia, South America, Cenozoic continental plateau lavas of tholeiitic and alkaline affinities are widespread in the Andean extra back-arc region (34°S–52°S; Fig. 1) and have been the subject of many petrogenetic studies (e.g. Gorring & Kay 2001; D'Orazio *et al*. 2004; Kay *et al*. 2007; Bruni *et al*. 2008). The volcanic activity is associated with a series of ridge collisions along the Chile trench. At least two mid-ocean ridge systems collided with this part of western South America in the Paleocene–Eocene and the Neogene–Quaternary (Cande & Leslie 1986), producing voluminous lavas in northern Patagonia (34°S–46°S) during the earlier collision (Ramos & Kay 1992) and the plateau lavas of southern Patagonia (46°S–52°S) during the more recent collision (Gorring *et al*. 1997).

Magma genesis of the Cenozoic Patagonian basalts has been interpreted as the product of asthenospheric melts derived either from shallow asthenospheric mantle upwelling linked with slab window processes (e.g. Ramos & Kay 1992; Gorring *et al*. 1997; D'Orazio *et al*. 2000; Gorring & Kay 2001; Gorring *et al*. 2003; Espinoza *et al*. 2005) or from the thermal and mechanical perturbation of the lithospheric and/or asthenospheric mantle

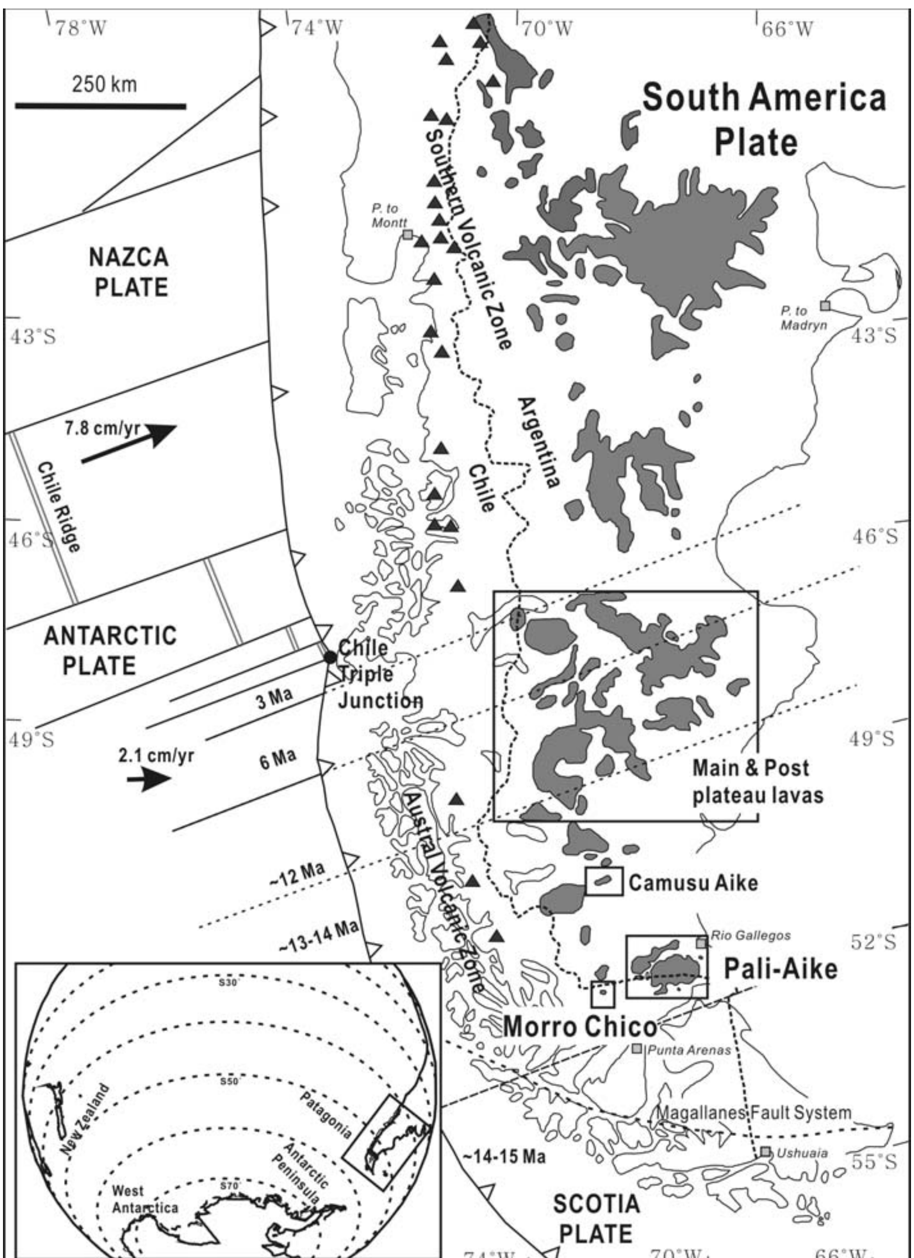

Fig. 1 Schematic geodynamic setting of southern South America and the adjacent Pacific Ocean. Lines under the Pacific Ocean are the fracture zones of the oceanic Nazca and Antarctic Plates (continuous lines), the Chile trench (continuous line with triangles on the overriding plate), and the transcurrent margin between the Scotia and South American Plates (dashed line). The black circle indicates the Chile Triple Junction. Black triangles indicate the main active volcanoes of the Austral Volcanic Zone and Southern Volcanic Zone, and gray areas mark the Cenozoic Patagonian plateau lavas. The two black arrows show convergence vectors of the Nazca and Antarctic Plates relative to South America (Gripp & Gordon, 2002). Numbers are the collision dates of ridges with the Chile trench (Cande & Leslie, 1986). Pali Aike (late Pliocene–Quaternary); Morro Chico (late Miocene); Camusu Aike volcanic field (late Pliocene); main and post Plateau lavas (late Miocene–Quaternary) are shown. Inset is a geographic map of southern South America, New Zealand and part of West Antarctica. Modified from Pankhurst *et al*. (1998), D'Orazio *et al*. (2001) and Ross *et al*. (2011).

caused by an abrupt change in subduction vectors or by reorganization of plates (e.g. Stern *et al.* 1990; De Ignacio *et al.* 2001; Motoki *et al.* 2005; Kay *et al.* 2007; Bruni *et al.* 2008). Another possible model is the microplume hypothesis (Kay *et al.* 1992). Although a variety of tectonic conditions could explain the volcanic activities in this region, there is increasing acceptance that the widespread Cenozoic back-arc volcanism in Patagonia has involved partial melting of shallow, upwelling asthenospheric mantle beneath an active continental margin. Compared to magmatism in the northern sector of extra-Andean Patagonia (34°S–45°S), the southernmost occurrences of this magmatism (46°S–52°S) have been studied in much better detail, yielding many possible geodynamic models. These models are, however, not relevant to the evolution of asthenospheric mantle beneath southern Patagonia in the middle to late Miocene.

Recent geochemical studies of mafic magmas derived from continental extension zones have successfully documented the nature of asthenospheric mantle (Lum *et al.* 1989; Liu *et al.* 1994; Choi *et al.* 2006). Neogene slab window lavas from Baja California to British Columbia on the western North American continental margin have mid-ocean ridge basalt (MORB)-like depleted signatures (Storey *et al.* 1989; Thorkelson & Taylor 1989; Cole & Basu 1995; Luhr *et al.* 1995). In contrast, slab window lavas from the Antarctic Peninsula show a high-μ (HIMU)-like mantle signature (high $^{238}U/^{204}Pb$). Previous studies of Patagonian extra-back-arc lavas have shown wide chemical and isotopic variability, ranging from signatures of an enriched ocean island basalt (OIB)-like mantle source to HIMU-like mantle (e.g. Gorring & Kay 2001; D'Orazio *et al.* 2004; Kay *et al.* 2007; Bruni *et al.* 2008).

This paper uses major and trace element geochemistry and Sr–Nd–Pb isotope composition to assess the relative contributions of different components and variable degrees of partial melting in the generation of Cenozoic plateau lavas from the Pali Aike volcanic field and Morro Chico volcano, the southernmost exposures of volcanic rock in Patagonia (51°S–52°S; Figs 1,2), and to evaluate the nature of their mantle source. Their chemistry indicates that the asthenospheric mantle beneath the Pali Aike and Morro Chico is relatively depleted and has a HIMU-like mantle signature. This characteristic is similar to that of slab window lavas from the Antarctic Peninsula, south of the study area, but quite different from those of southern Patagonian lavas between 46°S and 50°S to the north of the Pali Aike and Morro Chico. Together with published data, the spatiotemporal variation in chemical and isotopic characteristics of the Cenozoic Patagonian plateau lavas in the southern sector of extra-Andean Patagonia are traced to constrain asthenospheric mantle source heterogeneities and to discuss the origin of the HIMU-like mantle signature of the Pali Aike and Morro Chico lavas. A possible link between the HIMU-like mantle signature of the Pali Aike and Morro Chico and the HIMU mega-province of the southwestern Pacific is discussed.

REGIONAL GEOLOGY AND PETROGRAPHY

Miocene to Holocene plateau volcanic fields are exposed over large areas (46.5°S–52°S) of the southern Andean back-arc in southern Patagonia, where the South American, Nazca, Antarctic, and Scotia Plates interact (Fig. 1). The main geodynamic factors responsible for the tectonic evolution of this region are subduction of the South Chile spreading ridge, which separated the Nazca Plate from the Antarctic Plate, beneath the South American Plate, and transcurrent movement along the boundary between the Scotia and South American Plates.

The initial collision of the Chile Ridge with the Chile Trench started at 15–14 Ma in the southern tip of Patagonia (Cande & Leslie 1986), forming a triple junction between the South American, Nazca, and Antarctic Plates. The Chile Triple Junction has since migrated northward to its present position (~46°S) as a result of the oblique collision between the ridge and trench (Cande & Leslie 1986; Tebbens & Cande 1997; Tebbens *et al.* 1997). Transcurrent movements along the northern margin of the Scotia Plate strongly deformed the southernmost tip of South America, and have been related to the tectonic regime of this region, which was predominantly convergent until the late Miocene (Klepeis 1994; D'Orazio *et al.* 2000).

A series of Neogene ridge collisions resulted in upwelling of underlying asthenospheric mantle through a slab window, which produced the extensive Late Miocene to Holocene plateau lavas of the southern Patagonian back-arc region (e.g. Ramos & Kay 1992; D'Orazio *et al.* 2000; Gorring & Kay 2001). These lavas are most abundant between 46°S and 50°S, over the northeastern part of the ridge segment that collided at *ca* 12 Ma (Fig. 1).

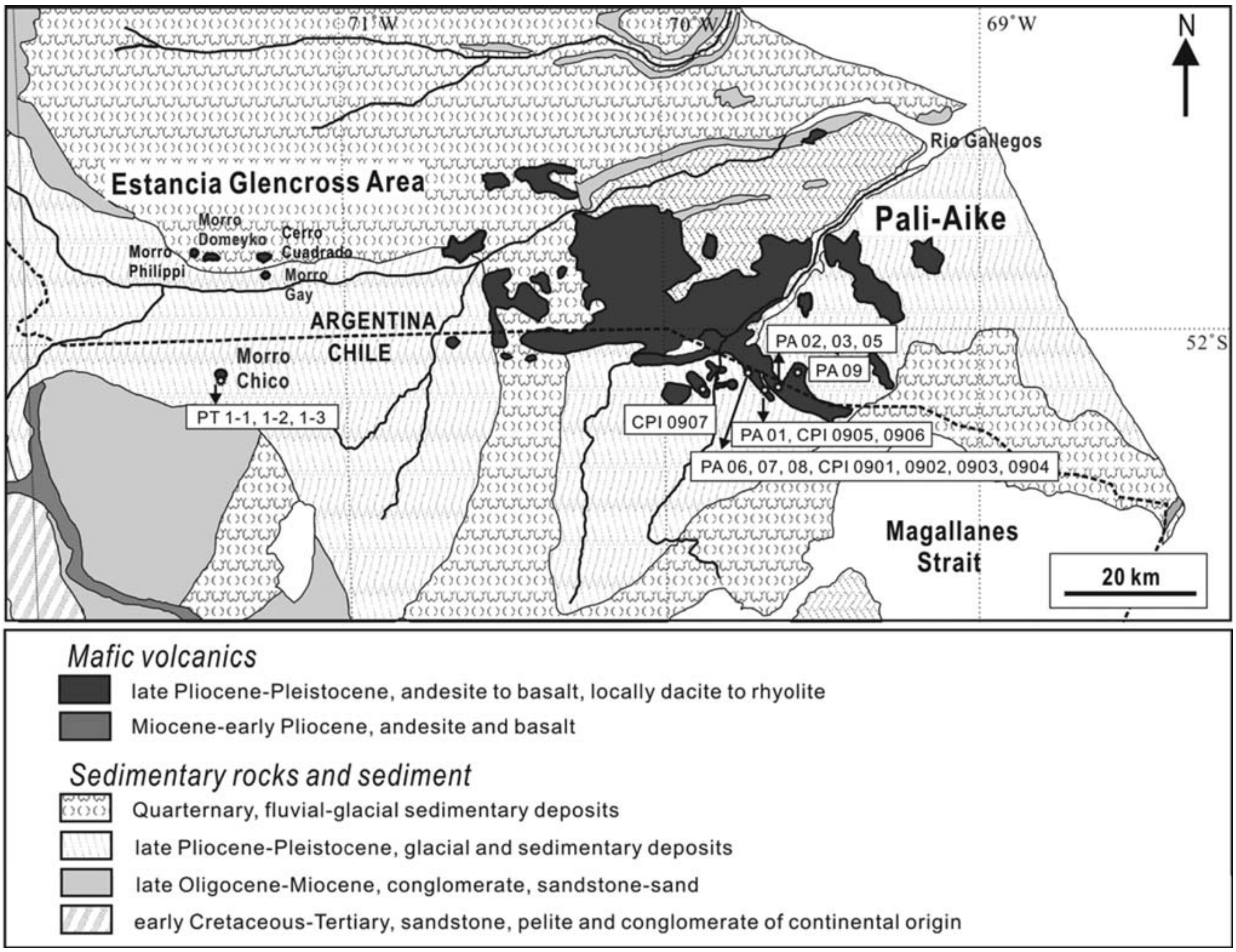

Fig. 2 Geological map showing sample locations in the Pali Aike and Morro Chico lavas.

Gorring and Kay (2001) subdivided these lavas into: (i) voluminous, late Miocene to early Pliocene (12–5 Ma) main plateau lavas; and (ii) younger, less voluminous, latest Miocene to Pleistocene (7–2 Ma) post-plateau lavas.

South of the voluminous main plateau lavas, volcanic rocks of the Pali Aike erupted along a northern part of the major strike-slip Magellan Fault Zone. The Morro Chico volcano is situated about 50 km west of the westernmost plateau lavas of the Pali Aike volcanic field (Fig. 2). The Camusu Aike volcanic field lavas are about 200 km northwest of the Pali Aike volcanic field, in the area between the main southern Patagonian slab window lavas (46.5°S and 49.5°S) and the Pali Aike lavas. Ages of the Camusu Aike lavas range from 2.9 to 2.5 Ma (D'Orazio *et al.* 2005) and are much younger than those of most of the southern Patagonian slab window lavas (46.5°S and 49.5°S) (Gorring *et al.* 1997, 2003; Gorring & Kay 2001).

Slab window lavas in southern Patagonia young to the northeast, with ages ranging from *ca* 12 Ma to Recent, following the track of subducted ridges. The Pali Aike Volcanic Field is the southernmost plateau basalt field, covering 4500 km^2, and is young (3.8 Ma to recent based on K–Ar and $^{40}Ar/^{39}Ar$ age data, Mercer 1976; Linares & Gonzalez 1990; Meglioli 1992; Singer *et al.* 1997; Corbella 1999). The time delay relative to subduction has been explained by the hypothesis that an extensional tectonic regime developed in the Pali Aike area only after 8–6 Ma (D'Orazio *et al.* 2000).

In general, the Pali Aike basalts have porphyritic textures, with olivine phenocrysts that have chrome-spinel inclusions, and clinopyroxene and plagioclase in an intergranular groundmass (D'Orazio *et al.* 2000). Interactions between olivine phenocrysts and the groundmass have not been documented, and plagioclase phenocrysts are rare.

The groundmass consists of olivine, clinopyroxene, plagioclase microlites, alkali feldspar, and titaniferous magnetite.

The Morro Chico volcano is one of five volcanic edifices of the Estancia Glencross area at the western end of the Rio Gallegos valley (52°S; Fig. 2) and, like the Pali Aike volcanic field, is related to Miocene ridge collisions. Exposures of the Morro Chico volcano form a series of five conspicuous buttes in the Estancia Glencross area: Morro Philippi, Morro Chico, Morro Domeyko, Morro Gay, and Cerro Cuadrado. The Morro Chico lavas in the study area are subalkaline. Their emplacement predates that of the Pali Aike lavas by 4–8 m.y. but postdates by 4 m.y. the main plateau lavas farther to the north (Gorring *et al.* 1997; D'Orazio *et al.* 2001). The Morro Chico lavas provide an opportunity to investigate spatiotemporal geochemical variation in the southernmost Patagonia lavas and to constrain related spatial variation in the nature of asthenospheric mantle.

The Morro Chico lavas have a porphyritic–glomeroporphyritic texture with a phenocryst assemblage composed of olivine, clinopyroxene, and traces of plagioclase in an intergranular groundmass. The groundmass consists of plagioclase microlites, clinopyroxene, Fe–Ti oxide, rare alkali feldspar, and interstitial glass. Millimeter-sized quartz aggregates considered to be microxenoliths and isolated quartz xenocrysts are locally present in Morro Chico basalt (D'Orazio *et al.* 2001).

ANALYTICAL METHODS

Twenty-six samples (23 from Pali Aike and 3 from Morro Chico) were selected for whole-rock and isotope analyses. Samples for the whole-rock analysis were prepared from rock fragments free of any visible weathering surfaces. The rock samples were crushed to <1 cm size and pulverized in an agate ball mill (Retsch PM400). This produced about 20–30 g of powdered material for each sample.

Major elements were analyzed by X-ray fluorescence (XRF) spectrometry using a Shimadzu XRF-1700 at the Cooperative Laboratory Center, Pukyong National University, Korea, following the method described by Kim *et al.* (2009). Trace element concentrations were determined by solution measurements on an inductively coupled plasma–mass spectrometer (ICP-MS, Perkin Elmer Elan 6100) at the Korea Polar Research Institute (KOPRI). Values for standards (BHVO-2, JB-2, and JB-3) that were analyzed at the same time as the study materials are reported with the main results in Tables 1 and 2. Samples (0.1 g) were dissolved in a mixture of ultra-pure, concentrated $HF–HNO_3–HClO_4$ for the ICP-MS analysis. Precision was estimated to be within 5% for major and trace elements by the XRF and ICP-MS analyses. Accuracy is estimated better than 5% for most trace elements by analyses of the BHVO-2, JB-2 and JB-3 standards.

Chemical separation and mass spectrometry for Sr, Nd, and Pb isotope analyses were performed at KOPRI. The analytical procedures were the same as those reported by Lee *et al.* (2011). The mass spectrometric analysis for Sr, Nd, and Pb isotopes was performed on a thermal ionization mass spectrometer (TIMS, Thermo Finnigan, Triton) equipped with nine adjustable Faraday cups. Sr and Nd isotopic compositions were measured in static mode with relay matrix rotation (the 'virtual amplifier' of Finnigan) on single Ta and double Re filaments, respectively. The data were corrected for mass fractionation by normalizing to $^{86}Sr/^{88}Sr = 0.1194$ and $^{146}Nd/^{144}Nd = 0.7219$, using an exponential law. Replicate analyses of NBS 987 and La Jolla standards gave $^{87}Sr/^{86}Sr = 0.710260 \pm 4$ ($n = 20$, 2σ) and $^{143}Nd/^{144}Nd = 0.511847 \pm 1$ ($n = 17$, 2σ). Samples for Pb isotope analysis were loaded on a single Re filament with silica gel and 0.1 M H_3PO_4, and the data were corrected for instrumental mass fractionation using the values of Todt *et al.* (1996) for the NBS 981 standard. Replicate analyses of the NBS 981 standard gave values of 36.486 ± 0.016, 15.422 ± 0.005, and 16.885 ± 0.005 for $^{208}Pb/^{204}Pb$, $^{207}Pb/^{204}Pb$, and $^{206}Pb/^{204}Pb$, respectively (mean, 2σ, $n = 28$). Total blanks averaged were 0.3 ng for Sr, 0.01 ng for Nd, and 0.5 ng for Pb. Considering that the procedural chemistry blanks in all cases were less than 0.5% of the sample amount, and the isotope ratios of blanks were not significantly different from those of analyzed samples, the influence of the blanks on the isotope ratios of the samples is negligible within the analytical error ranges. The results are given in Table 3.

RESULTS

MAJOR AND TRACE ELEMENTS

Table 2 lists the major and trace element concentrations of the Pail Aike and Morro Chico samples.

Table 1 Measured and certified values of major and trace element concentrations for international standards

	BCR-2			JB-2			JB-3			BHVO-2			
	M.V.	†R.V.[a]	R.D. %	M.V.	†R.V.[a]	R.D. (%)	M.V.	†R.V.[a]	R.D. (%)	M.V.	†R.V.[a]	†R.V.[b]	R.D. (%)
SiO_2 (wt.%)	54.04	54.1 ± 0.8	0.1										
Al_2O_3	13.38	13.5 ± 0.2	0.6										
TiO_2	2.25	2.26 ± 0.05	0.3										
Fe_2O_3	13.82	13.8 ± 0.2	0.2										
MnO	0.19	0.196 ± 0.008	0.6										
MgO	3.53	3.59 ± 0.05	0.3										
CaO	7.06	7.12 ± 0.11	0.8										
Na_2O	2.99	3.16 ± 0.11	2.0										
K_2O	1.80	1.79 ± 0.05	0.7										
P_2O_5	0.34	0.35 ± 0.02	2.8										
La (ppm)				2.40	2.35 ± 0.23	2.3	8.98	8.81 ± 0.77	1.9	15.94	15 ± 1	15.4 ± 0.5	0.3
Ce				6.88	6.76 ± 0.95	1.8	22.40	21.5 ± 1.7	3.4	38.92	38 ± 2	37.8 ± 1.4	0.7
Pr				1.30	1.01 ± 0.26	2.1	3.49	3.26 ± 0.42	5.2	5.92		5.35 ± 0.17	7.3
Nd				6.95	6.63 ± 0.7	4.8	16.31	15.6 ± 2.1	4.6	26.36	25 ± 1.8	24.6 ± 0.9	3.4
Sm				2.50	2.31 ± 0.37	3.9	4.49	4.27 ± 0.24	0.4	6.54	6.2 ± 0.4	6.12 ± 0.21	0.9
Eu				0.96	0.86 ± 0.07	2.8	1.42	1.32 ± 0.12	1.2	2.27		2.06 ± 0.07	6.7
Gd				3.30	3.28 ± 0.31	0.5	4.85	4.67 ± 0.64	3.9	6.74	6.3 ± 0.2	6.22 ± 0.26	3.7
Tb				0.63	0.6 ± 0.1	0.4	0.79	0.730 ± 0.087	3.3	1.05	0.90	0.96 ± 0.04	5.2
Dy				4.38	3.73 ± 0.59	1.3	4.95	4.54 ± 0.37	0.7	5.97		5.36 ± 0.23	6.8
Ho				0.95	0.75 ± 0.17	3.7	0.99	0.80 ± 0.15	3.9	1.06	1.04 ± 0.04	0.98 ± 0.03	1.9
Er				2.84	2.6 ± 0.3	2.0	2.88	2.49 ± 0.45	1.9	2.83		2.57 ± 0.10	6.1
Tm				0.42	0.41 ± 0.1	2.6	0.41	0.420 ± 0.051	3.4	0.36		0.33 ± 0.01	6.3
Yb				2.75	2.62 ± 0.4	3.5	2.64	2.55 ± 0.47	3.4	2.19	2 ± 0.2	1.98 ± 0.08	0.3
Lu				0.44	0.4 ± 0.06	4.7	0.41			0.32	0.28 ± 0.01	0.28 ± 0.01	9.1
Sc				58.72	53.5 ± 6.6	2.3	35.99			33.60		31.4 ± 0.7	4.7
Th				0.30	0.35 ± 0.17	0.1	1.44			1.40	1.2 ± 0.3	1.22 ± 0.06	6.9
U				0.18	0.18 ± 0.067	2.3	0.53	0.480 ± 0.087	5.6	0.48		0.41 ± 0.02	11.2
Y				23.55	24.9 ± 3.1	5.4	25.25	26.9 ± 3.0	6.1	26.00		25.8 ± 0.8	0.8
Hf				1.70	1.49 ± 0.31	5.5	2.93	2.67 ± 0.12	5.0	4.99		4.52 ± 0.21	5.5
Mo				0.62	1.08 ± 0.47	1.1	1.19	1.09 ± 0.20	1.0	3.36		3.43 ± 0.52	2.0
Nb				0.47	1.58* ± 1.09	4.5	2.09	2.47 ± 0.85	0.0	18.83	18 ± 2	18.5 ± 0.8	0.9
Sn				0.60	0.95 ± 0.44	0.2	0.99	0.94 ± 0.14	5.3	1.87			
Ta				0.05	0.13 ± 0.067	8.0	0.14	0.150 ± 0.045	4.3	1.24	1.40	1.21 ± 0.05	1.6
Zr				49.05	51.2 ± 6.1	4.2	96.61	97.8 ± 7.4	1.2	176.87	172 ± 11	173 ± 5	0.6
Ba				243.84	222 ± 31	3.6	261.77	245 ± 26	3.4	140.98		132 ± 4	3.7
Pb				5.66	5.36 ± 1.08	5.6	5.47	5.58 ± 1.87	2.0	1.92		1.72 ± 0.26	2.9
Cs				0.85	0.85 ± 0.2	0.6	1.00	0.94 ± 0.21	6.4	0.10		0.09 ± 0.01	3.7
Li				8.92	7.78 ± 1.39	2.8	7.83	7.21 ± 1.13	6.1	4.75			
Rb				6.23	7.37 ± 2.89	2.2	15.00	15.1 ± 2.3	0.7	9.53		9.07 ± 0.25	2.2
Sr				194.21	178 ± 19	1.4	430.15	403 ± 36	2.0	421.55		393 ± 16	3.3
Co				40.66	38 ± 6.6	7.0	38.02	34.3 ± 5.5	4.5	48.08		45.1 ± 1	6.6
Cu				222.28	225 ± 16	1.2	192.70	194 ± 16	0.7	132.63		128 ± 4	0.5
Ni				15.22	16.6 ± 6.7	8.3	38.75	36.2 ± 6.1	7.0	118.28		120 ± 3	1.4

† R.V.[a]: Certified values of United States Geological Survey; R.V.[b]: Trace elements values were determined by LA-ICP-MS (McCoy-West *et al.* 2010).
M.V., measured value; R.V., recommended value; R.D, relative deviation in %, |M.V.-R.V.|/R.V. \ 100.

Table 2 Major and trace element compositions of the Pali Aike and Morro Chico lavas

	Pali Aike												
Sample	PA01-5	PA02-3	PA2801	PA03	PA05-1	PA05-2	PA05-3	PA06	PA07	PA09-2	PA09-3	PA09-4	PA09-05-1
Latitude (S)	52°06′66″	52°06′43″	52°06′66″	52°06′58″	52°06′57″	52°06′57″	52°06′57″	52°04′93″	52°04′78″	52°04′59″	52°04′52″	52°04′52″	52°04′52″
Longitude (W)	69°42′49″	69°40′57″	69°42′49″	69°40′37″	69°40′23″	69°40′23″	69°40′23″	69°47′13″	69°47′09″	69°34′78″	69°35′05″	69°35′05″	69°35′05″
Rock type	Ba	Ba	Tb	Ba	Ba	Ba	Ba	Ba	Ba	Tb	Tb	Tb	Ba
Major elements (wt.%)													
SiO_2	46.34	46.22	45.43	46.39	46.45	46.80	46.47	46.40	46.30	45.43	45.36	46.31	45.68
TiO_2	2.74	2.73	2.84	2.78	2.80	2.78	2.76	2.51	2.52	3.10	3.13	3.30	3.24
Al_2O_3	11.05	11.57	10.10	11.83	11.64	11.69	11.44	11.19	11.39	10.52	10.51	10.97	10.48
Fe_2O_3	12.68	12.75	12.32	12.55	12.86	12.85	12.73	12.46	12.41	13.07	12.97	13.00	13.25
MnO	0.15	0.15	0.16	0.15	0.16	0.16	0.15	0.16	0.16	0.16	0.16	0.16	0.16
MgO	12.29	10.97	13.65	10.20	10.49	10.53	10.38	11.27	11.32	12.09	12.02	11.08	11.73
CaO	9.83	9.98	10.04	10.27	10.12	10.07	9.87	11.01	10.84	9.71	9.73	9.92	9.89
Na_2O	3.16	3.41	2.85	3.45	3.24	3.23	3.16	3.00	3.17	3.43	3.48	3.06	3.25
K_2O	1.24	1.48	1.45	1.51	1.49	1.50	1.49	1.23	1.26	1.66	1.69	1.74	1.68
P_2O_5	0.54	0.63	0.63	0.61	0.60	0.60	0.58	0.53	0.55	0.72	0.74	0.77	0.73
LOI†	0.15	0.03	0.24	0.01	−0.22	−0.25	0.30	−0.11	0.06	0.02	0.02	−0.55	−0.31
Total	100.2	99.9	99.7	99.8	99.6	100.0	99.3	99.7	100.0	99.9	99.8	99.8	99.8
Mg#‡	69.3	66.7	72.1	65.4	65.5	65.6	65.5	67.8	68.0	68.3	68.3	66.5	67.4
Trace elements (ppm)													
La	34.7	29.9	34.0	33.9	30.8	30.5	29.9	32.1	32.5	39.8	40.9	42.1	36.2
Ce	69.2	62.1	68.5	69.3	63.8	63.1	62.3	63.2	64.3	88.2	83.1	93.8	69.9
Pr	9.9	8.6	9.6	9.6	8.3	8.3	8.1	8.1	8.8	11.1	11.6	11.9	10.6
Nd	41.2	35.8	39.8	39.8	34.1	34.8	34.0	32.7	36.0	45.9	47.5	48.5	40.3
Sm	9.00	8.10	8.65	8.96	7.76	7.88	7.72	7.38	8.04	10.11	10.48	10.67	9.05
Eu	2.89	2.66	2.82	2.93	2.66	2.65	2.63	2.56	2.69	3.38	3.38	3.54	3.05
Gd	8.65	7.90	8.29	8.61	7.78	7.81	7.75	7.63	7.99	10.22	10.02	10.84	9.21
Tb	1.13	1.07	1.10	1.18	1.07	1.07	1.07	1.04	1.09	1.46	1.33	1.55	1.22
Dy	5.81	5.58	5.55	6.15	5.49	5.54	5.60	5.33	5.70	7.06	6.75	7.43	6.18
Ho	0.94	0.91	0.89	1.01	0.92	0.94	0.93	0.91	0.94	1.14	1.08	1.20	0.99
Er	2.47	2.40	2.30	2.63	2.37	2.40	2.35	2.36	2.45	3.02	2.76	3.10	2.60
Tm	0.26	0.26	0.24	0.29	0.28	0.28	0.28	0.28	0.27	0.32	0.29	0.34	0.30
Yb	1.66	1.66	1.58	1.82	1.67	1.68	1.71	1.65	1.75	2.05	1.84	2.11	1.79
Lu	0.20	0.20	0.19	0.22	0.23	0.24	0.23	0.24	0.22	0.27	0.22	0.29	0.23
Sc	21.61	22.88	22.24	22.50	23.47	23.70	23.11	24.28	23.56	25.34	22.30	25.27	20.35
Th	4.20	3.49	3.88	3.98	3.44	3.64	3.52	3.72	3.84	4.83	4.38	5.14	3.48
U	1.08	1.04	1.08	1.18	1.05	1.12	1.04	0.91	0.94	1.47	1.29	1.39	1.04
Y	23.96	23.16	23.34	25.72	23.91	23.34	24.35	23.85	24.61	28.65	27.86	29.74	23.92
Hf	5.19	5.05	5.00	5.45	5.07	5.13	5.04	4.18	4.37	7.17	6.55	7.69	5.67
Mo	1.74	3.22	2.17	3.62	3.23	3.22	2.99	2.32	2.37	4.15	3.89	3.58	3.18
Nb	48.9	44.1	51.2	51.4	48.1	46.5	47.4	48.9	48.9	59.3	58.8	61.1	45.8
Sn	1.81	1.93	1.95	2.18	1.97	1.95	1.97	1.83	1.80	2.18	2.37	2.36	2.19
Ta	2.70	2.36	2.74	2.85	2.60	2.56	2.54	2.36	2.49	3.89	3.31	4.10	2.79
W	0.44	0.69	0.70	1.15	1.55	1.38	1.58	0.94	0.58	1.96	0.83	2.54	1.60
Zr	219	215	213	230	222	218	224	181	182	304	277	317	206
Ba	464	394	459	444	403	397	400	437	449	497	484	538	411
Pb	2.39	2.26	2.21	2.69	2.30	2.49	2.45	2.08	2.16	2.77	2.52	2.99	2.38
Cs	0.38	0.37	0.26	0.38	0.43	0.33	0.35	0.27	0.30	0.33	0.40	0.31	0.39
Li	6.59	6.44	6.11	6.91	6.85	7.12	6.68	6.32	6.08	8.80	6.79	9.69	5.87
Rb	26.4	24.0	23.8	27.6	24.0	24.1	25.0	21.7	22.4	30.0	30.8	31.3	23.5
Sr	736	660	723	720	683	683	676	697	700	804	788	857	641
Co	64	58	65	47	59	58	59	61	58	65	63	64	60
Cr	443	192	209	291	298	347	304	251	247	199	195	393	294
Cu	61	54	60	66	54	56	59	55	53	78	71	75	58
Ni	399	256	411	146	262	259	260	260	240	341	326	305	262

Table 2 *Continued*

	Pali Aike									Morro Chico		
Sample	PA09-05-2	CPI0901	CPI0902	CPI0903	CPI0904	CPI0904-1	CPI0905	CPI0906-1	CPI0907	PT1-1	PT1-2	PT1-3
Latitude (S)	52°04′52″	52°04′44″	52°04′44″	52°04′37″	52°04′42″	52°06′35″	52°06′36″	52°06′36″	52°07′33″	52°03′47″	52°03′47″	52°03′47″
Longitude (W)	69°35′05″	69°47′08″	69°47′08″	69°46′32″	69°46′44″	69°42′25″	69°42′00″	69°42′00″	69°52′04″	71°25′38″	71°25′38″	71°25′38″
Rock type	Ba	Ba	Ba	Ba	Ba	Ba	Ba	Ba	Ba	Ba	Ba	Ba
Major elements (wt.%)												
SiO_2	45.99	46.66	46.60	48.48	46.64	45.87	46.82	46.85	45.43	50.51	50.67	50.80
TiO_2	3.17	2.57	2.53	2.80	2.57	2.51	2.87	2.79	2.67	2.69	2.77	2.81
Al_2O_3	10.63	11.42	11.33	12.44	11.60	11.24	10.24	11.64	10.95	12.32	12.66	12.73
Fe_2O_3	13.16	12.48	12.39	11.71	12.38	12.26	12.39	12.85	12.20	11.42	11.28	11.11
MnO	0.16	0.16	0.16	0.14	0.16	0.15	0.14	0.16	0.15	0.14	0.14	0.13
MgO	11.55	10.94	10.94	8.37	10.55	10.74	10.21	10.54	10.96	8.80	8.00	7.63
CaO	9.83	10.92	10.89	10.54	10.68	10.75	10.07	10.10	12.06	8.87	9.05	9.09
Na_2O	3.21	3.16	3.18	3.32	3.54	3.15	3.00	3.18	3.44	3.25	2.88	2.91
K_2O	1.66	1.27	1.28	1.39	1.39	1.26	1.50	1.50	1.21	1.14	1.07	1.24
P_2O_5	0.73	0.54	0.56	0.58	0.58	0.58	1.16	0.60	0.72	0.47	0.47	0.48
LOI†	-0.46	-0.06	-0.06	-0.12	–0.34	1.23	0.98	-0.34	-0.15	0.59	0.88	0.80
Total	99.6	100.1	99.8	99.6	99.7	99.7	99.4	99.9	99.6	100.2	99.9	99.7
Mg#‡	67.2	67.1	67.3	62.5	66.5	67.1	65.8	65.7	67.7	64.2	62.3	61.6
Trace elements (ppm)												
La	47.4	33.1	33.0	28.8	34.6	33.0	36.3	30.7	48.8	24.9	25.6	25.9
Ce	91.9	65.3	65.5	59.9	68.1	63.4	72.0	63.9	87.9	51.9	53.1	54.1
Pr	13.7	8.2	8.3	7.7	8.7	8.2	9.3	8.2	10.5	7.3	7.5	7.5
Nd	50.8	33.5	33.4	32.4	35.4	33.4	38.6	34.5	41.1	31.4	32.2	32.2
Sm	10.99	7.44	7.38	7.69	7.88	7.44	8.37	7.83	8.43	7.68	7.81	7.95
Eu	3.60	2.56	2.52	2.59	2.67	2.55	2.78	2.63	2.87	2.61	2.75	2.76
Gd	11.26	7.60	7.52	7.77	8.04	7.48	8.19	7.69	8.60	7.45	8.07	8.06
Tb	1.42	1.05	1.04	1.09	1.08	1.04	1.09	1.06	1.13	1.06	1.21	1.21
Dy	7.16	5.42	5.62	5.73	5.65	5.50	5.48	5.56	5.67	5.50	6.02	6.02
Ho	1.13	0.91	0.95	0.99	0.93	0.94	0.92	0.92	0.93	0.91	1.01	1.02
Er	2.91	2.36	2.44	2.55	2.44	2.46	2.32	2.36	2.39	2.36	2.68	2.66
Tm	0.33	0.28	0.29	0.30	0.30	0.30	0.28	0.28	0.28	0.26	0.30	0.30
Yb	1.94	1.72	1.74	1.85	1.76	1.77	1.61	1.65	1.67	1.68	1.90	1.90
Lu	0.25	0.24	0.24	0.26	0.25	0.25	0.22	0.23	0.23	0.20	0.26	0.26
Sc	19.60	23.35	23.45	24.31	23.06	22.64	22.20	23.75	23.39	20.50	23.40	23.69
Th	4.41	3.97	3.88	3.84	4.09	3.92	4.12	3.68	6.72	3.25	3.75	3.85
U	1.26	1.01	1.05	1.07	1.07	1.06	0.89	1.12	1.67	0.93	1.11	1.12
Y	27.44	22.93	24.62	25.59	25.06	24.19	24.43	23.35	24.17	23.01	25.60	25.82
Hf	7.18	4.31	4.27	4.94	4.38	4.16	5.06	5.05	4.11	4.74	5.81	5.81
Mo	3.75	2.48	2.88	2.77	2.54	2.38	1.83	3.21	4.08	2.20	2.88	2.71
Nb	57.1	48.0	49.3	43.9	54.2	45.2	55.2	46.1	61.3	32.3	36.3	36.4
Sn	2.63	1.70	1.72	2.04	1.81	1.62	1.98	1.90	1.72	1.85	1.86	1.81
Ta	3.51	2.49	2.40	2.40	2.60	2.27	2.85	2.49	2.56	1.89	2.55	2.47
W	1.33	0.78	1.17	0.87	0.88	1.00	1.08	1.15	1.45	0.56	1.46	2.28
Zr	269	171	186	208	197	171	230	221	180	196	221	224
Ba	486	500	442	388	467	444	488	404	623	286	312	318
Pb	2.78	2.27	2.23	2.72	2.38	2.21	2.32	2.51	3.31	3.11	3.54	3.54
Cs	0.50	0.28	0.27	0.43	0.31	0.26	0.31	0.32	0.27	0.44	0.45	0.44
Li	6.18	6.96	6.69	6.64	6.80	6.21	5.59	7.00	7.47	7.26	9.91	9.48
Rb	29.3	20.7	21.8	26.4	24.9	20.9	26.0	23.5	19.0	19.2	19.5	21.7
Sr	717	758	681	657	718	674	770	676	898	631	678	678
Co	64	58	59	49	57	57	59	59	61	47	48	46
Cr	381	289	292	436	195	285	292	295	381	378	320	147
Cu	73	50	58	44	54	50	57	58	71	53	63	64
Ni	329	241	247	162	241	238	353	262	264	210	202	187

† L.O.I., loss on ignition.
‡ Mg# = 100Mg/(Mg + Fe^{2+}), assuming Fe_2O_3/FeO = 0.15 ; Ba, basalt; Tb, trachybasalt.

Table 3 Sr, Nd, and Pb isotope data for the Pali Aike and Morro Chico lavas

	Sample name	$^{87}Sr/^{86}Sr$	$^{143}Nd/^{144}Nd$	εNd†	$^{206}Pb/^{204}Pb$	$^{207}Pb/^{204}Pb$	$^{208}Pb/^{204}Pb$	Δ7/4‡	Δ8/4‡
Pali Aike	CPI0901	0.703511 ± 12	0.512916 ± 6	5.4	18.871 ± 0.013	15.631 ± 0.011	38.683 ± 0.027	9.4	24.1
	CPI0906-1	0.703399 ± 9	0.512905 ± 5	5.2	18.939 ± 0.013	15.636 ± 0.011	38.727 ± 0.027	9.2	20.2
	CPI0907	0.703325 ± 12	0.512920 ± 5	5.5	18.790 ± 0.006	15.596 ± 0.006	38.573 ± 0.013	6.8	22.8
	PA01-5	0.703421 ± 13	0.512915 ± 4	5.4	19.015 ± 0.014	15.655 ± 0.012	38.759 ± 0.029	10.3	14.2
	PA02-3	0.703433 ± 11	0.512901 ± 5	5.1	18.965 ± 0.009	15.648 ± 0.007	38.791 ± 0.019	10.2	23.5
	PA05-2	0.703404 ± 11	0.512904 ± 6	5.2	18.932 ± 0.014	15.641 ± 0.011	38.748 ± 0.028	9.8	23.3
	PA06	0.703272 ± 9	0.512923 ± 3	5.6	18.922 ± 0.021	15.649 ± 0.018	38.748 ± 0.046	10.7	24.4
	PA09-3	0.703320 ± 8	0.512883 ± 3	4.8	19.168 ± 0.010	15.663 ± 0.007	38.905 ± 0.020	9.4	10.4
	PA09-4	0.703341 ± 10	0.512887 ± 8	4.9	19.158 ± 0.005	15.643 ± 0.004	38.864 ± 0.010	7.5	7.5
	PA09-05-1	0.703312 ± 10	0.512882 ± 2	4.8	19.170 ± 0.006	15.659 ± 0.005	38.909 ± 0.012	9.0	10.6
Morro Chico	PT1-1	0.703248 ± 6	0.512863 ± 6	4.4	18.942 ± 0.003	15.641 ± 0.003	38.781 ± 0.006	9.7	25.3
	PT1-2	0.703279 ± 15	0.512863 ± 8	4.4	18.945 ± 0.003	15.637 ± 0.002	38.773 ± 0.006	9.2	24.2
	PT1-3	0.703253 ± 7	0.512862 ± 7	4.4	18.970 ± 0.004	15.652 ± 0.003	38.823 ± 0.007	10.4	26.1

† εNd values were calculated using $\varepsilon Nd = [(^{143}Nd/^{144}Nd)_{sample}/(^{143}Nd/^{144}Nd)_{CHUR} - 1] \times 10^4$, where $(^{143}Nd/^{144}Nd)_{CHUR} = 0.512638$.
‡ Δ7/4Pb and Δ8/4Pb are computed as described by Hart (1984).

Previous data for the southern Patagonian slab window lavas are plotted together for comparison (Figs 3–5). The Pali Aike lavas show an alkaline basalt affinity (45–49 wt.% SiO_2; 3.5–6.0 wt.% Na_2O+K_2O) and plot in the fields of alkali basalt, trachybasalt, and basanite on a total alkali versus silica classification diagram (Fig. 3). In contrast, the Morro Chico lavas belong to the subalkaline series, plotting in a field of relatively high SiO_2 (50.5–50.8 wt.%) and moderate total alkalis (Na_2O+K_2O of 4.0–4.4 wt.%; Fig. 3). The compositions of the Pali Aike lavas are less alkaline (lower in both Na_2O and K_2O) than the Neogene southern Patagonian post-plateau lavas (46°S–50°S, Gorring & Kay 2001; Gorring *et al.* 2003) and are similar to those of alkali basalts from the Camusu Aike volcanic field (Fig. 3).

The Pali Aike lavas are quite primitive in composition, as indicated by relatively high Ni (147–400 ppm) and Cr (194–436 ppm), and high Mg# [= 100 Mg/(Mg+Fe^{2+})] that range from 62 to 73 (Table 1). The compositional ranges of Ni (187–210 ppm), Cr (147–378 ppm), and Mg# (62–64) of the Morro Chico lavas are similar to those of Pali Aike lavas.

Trace element compositions of the Pali Aike and Morro Chico lavas are compared on primitive-mantle-normalized multi-element variation plots (Sun & McDonough 1989; Fig. 4) with the southern Patagonian slab window lavas (Camusu Aike lavas, main and post-plateau lavas, Gorring & Kay 2001; Gorring *et al.* 2003; D'Orazio *et al.* 2005). The Pali Aike samples display higher concentrations of all incompatible trace elements compared to an average for OIB and have patterns that peak at Ba, Ta, and Nb (Sun & McDonough 1989; Fig. 4a). These enrichments are coupled with relative depletions of K, Pb, and Ti. The Pali Aike and Morro Chico samples show patterns that are similar to those of Coleman Nunatak and St Helena basalts, which are known as HIMU–OIB (Hart *et al.* 1997; Kawabata *et al.* 2011), but display different degrees of incompatible element enrichment owing to the slightly higher degrees of partial melting of the Morro Chico magma. The Pali Aike lavas are more enriched in light rare earth elements [LREE; $(La/Yb)_N = 11.2–21$ and $(Yb)_N = 3.4–4.3$)] than the subalkaline Morro Chico lavas [$(La/Yb)_N = 9.7–10.6$ and $(Yb)_N = 3.4–3.9$]. However, the rare earth element (REE) compositions of both the Pali Aike and Morro Chico samples indicate that they were derived by small melt fractions of a garnet-bearing source.

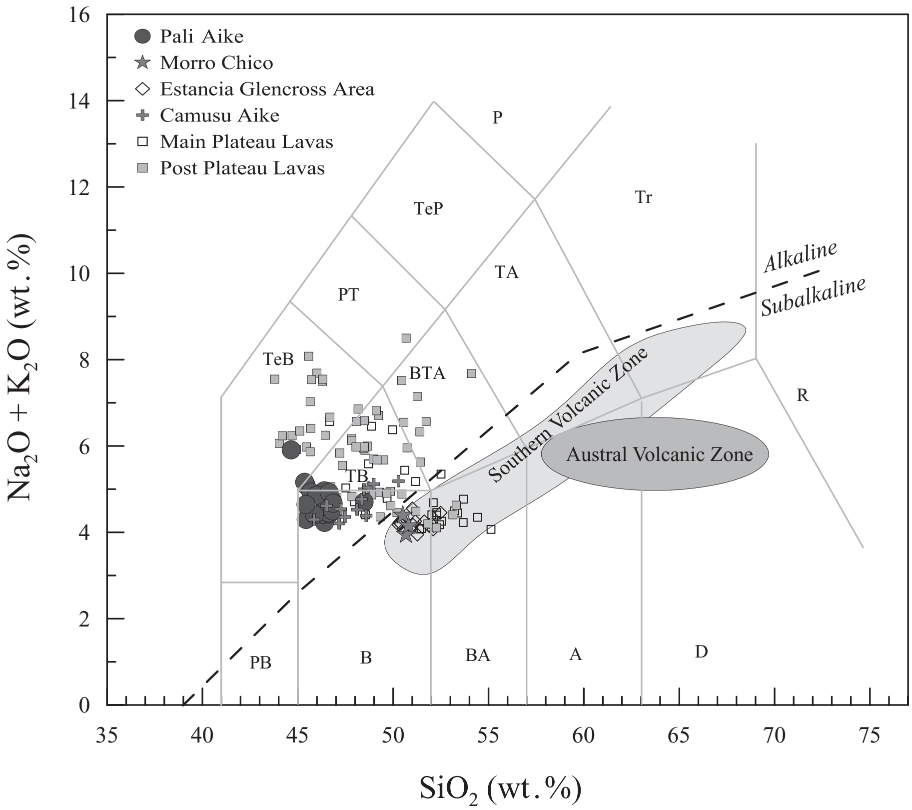

Fig. 3 Total alkalis *vs* silica classification diagram for the southern Patagonian basalts. Lines and fields are based on those of Le Bas *et al.* (1986). Compositional fields for the Southern volcanic zone and Austral Volcanic Zone basalts are shown. Data for the southern Patagonian slab window lavas are also plotted together for comparative purposes. Previous data sources are Hickey *et al.* (1986), Futa and Stern (1988), Stern and Kilian (1996), Gorring and Kay (2001), Gorring *et al.* (2003), and D'Orazio *et al.* (2001, 2005). PB, picrobasalt; B, basalt; BA, basaltic andesite; A, andesite; D, dacite; TB, trachybasalt; BTA, basaltic trachyandesite (mugearite); TA, trachyandesite; Tr, Trachyte; TeB, tephrite basanite; PT, phonotephrite; TeP, tephriphonolite; P, phonolite.

In spite of a wide compositional range of Neogene main plateau lavas in southern Patagonia, these rocks show an OIB-like signature that is enriched in large-ion lithophile elements (LILE) and LREE compared with normal mid-ocean ridge basalt (N-MORB) and relatively small depletions in high field-strength elements (HFSE) (Fig. 4b). Some of the main plateau lavas from the western region of the back-arc display small negative Nb and Ta anomalies, which indicate a minor influence of arc and/or continental crustal components (Fig. 4b). Most post plateau lavas in southern Patagonia have alkaline basalt affinities and their trace element patterns are similar to that of an average OIB (Fig. 4c). The Camusu Aike lavas exhibit slightly lower degrees of enrichment in incompatible elements than those of the Pali Aike and Morro Chico samples, but the trace element patterns of all three are similar (Fig. 4d).

Figure 5 shows the similarity of the Ba/La, La/Ta, Th/La, and Th/Nb ratios of southern Patagonian plateau lavas to global averages for alkali basalts. The Pali Aike and Morro Chico lavas have lower Ba/La, La/Ta, Th/Nb, and Th/La ratios than the other southern Patagonian slab window lavas. The compositional similarity between HIMU-like OIB and the Pali Aike, Morro Chico, and Camusu Aike lavas is also evident in these diagrams.

Sr, Nd, AND Pb ISOTOPES

The new Sr, Nd, and Pb isotope data for the Pali Aike and Morro Chico samples are presented in Table 3. Data were compared with results from the Neogene southern Patagonian plateau lavas and previously reported Pali Aike data (Stern *et al.* 1990; D'Orazio *et al.* 2000, 2005; Gorring & Kay 2001; Gorring *et al.* 2003) (Figs 6,7). The fields for the hypothetical mantle reservoirs depleted MORB mantle (DMM), HIMU, enriched mantle I (EMI), and enriched mantle II (EMII; Zindler & Hart 1986) are shown for comparison in these diagrams.

The Sr and Nd isotope data from the Pali Aike and Morro Chico lavas show relatively limited compositional variation, with low $^{87}Sr/^{86}Sr$ and high $^{143}Nd/^{144}Nd$ ratios (Pali Aike, $^{87}Sr/^{86}Sr = 0.703272$–$0.703511$, $^{143}Nd/^{144}Nd = 0.512882$–$0.512923$; Morro Chico, $^{87}Sr/^{86}Sr = 0.703248$–$0.703279$, $^{143}Nd/^{144}Nd = 0.512862$–$0.512863$). The signature of these lavas is markedly depleted relative to that of southern Patagonian plateau lavas, but their composition

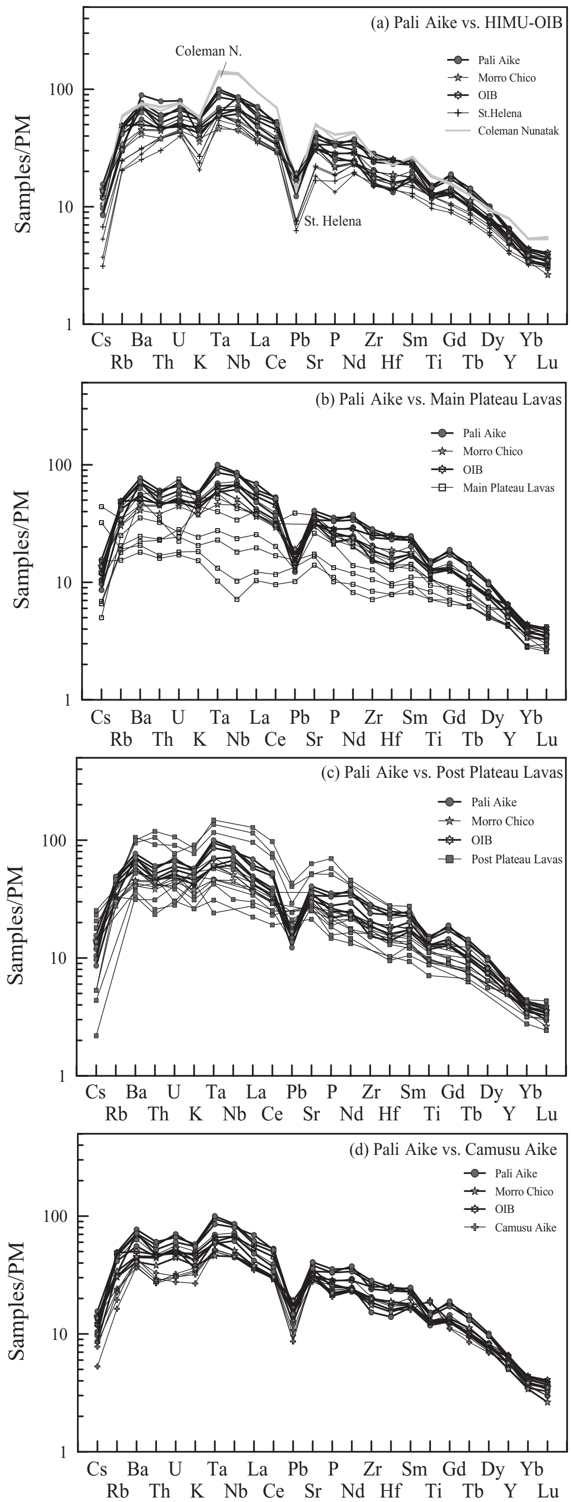

Fig. 4 Trace element patterns normalized to primitive mantle (Sun & McDonough 1989) for the Pali Aike and Morro Chico samples and some other southern Patagonian plateau basalts. Patterns of the studied samples from Pali Aike and Morro Chico and average OIB are compared with those of (a) representative HIMU–OIB, (b) main plateau lavas, (c) post-plateau lavas, and (d) Camusu Aike lavas. Data sources for comparison are (average oceanic island basalt (OIB), Sun and McDonough (1989); St Helena, Kawabata *et al.* (2011); Coleman Nunatak in Marie Byrd Land, Hart *et al.* (1997); Southern Patagonian lavas, Gorring and Kay (2001), Gorring *et al.* (2003), and D'Orazio *et al.* (2001, 2005).

partially overlaps with that of the Camusu Aike lavas (Fig. 6). The Sr–Nd isotopic compositions of the Pali Aike, Morro Chico, and Camusu Aike lavas plot within the range of HIMU-like slab window basalts from the Antarctic Peninsula.

The Pb isotope ratios of the Pali Aike and Morro Chico samples are relatively higher (Pali Aike $^{206}Pb/^{204}Pb = 18.871–19.170$, $^{207}Pb/^{204}Pb = 15.596–15.663$, and $^{208}Pb/^{204}Pb = 38.573–38.909$; Morro Chico $^{206}Pb/^{204}Pb = 18.942–18.970$, $^{207}Pb/^{204}Pb = 15.637–15.652$, and $^{208}Pb/^{204}Pb = 38.773–38.823$) than those of Neogene southern Patagonian post plateau lavas ($^{206}Pb/^{204}Pb = 18.208–18.699$, $^{207}Pb/^{204}Pb = 15.538–15.651$, and $^{208}Pb/^{204}Pb = 38.384–38.772$), and main plateau lavas ($^{206}Pb/^{204}Pb = 18.322–18.747$, $^{207}Pb/^{204}Pb = 15.569–15.643$, and $^{208}Pb/^{204}Pb = 38.212–38.700$) (Gorring & Kay 2001; Gorring *et al.* 2003). In plots of $^{207}Pb/^{204}Pb$ and $^{208}Pb/^{204}Pb$ versus $^{206}Pb/^{204}Pb$ (Fig. 7), the data from the Pali Aike and Morro Chico lavas form a linear array that extends into the field of HIMU-like OIB from New Zealand, the Antarctic Peninsula, and West Antarctica in the southwestern Pacific region, and plot above the Northern Hemisphere Reference Line (NHRL; Hart 1984). These diagrams demonstrate that Pb isotopic compositions of the southern Patagonian plateau basalts display a geographically controlled variation. Their $^{206}Pb/^{204}Pb$ ratios increase toward those of Neogene alkaline basalts at higher latitudes (50°S–52°S) in southern Patagonia, approximating a HIMU-like mantle signature.

DISCUSSION

CRUSTAL CONTAMINATION

The southern Patagonian plateau lavas were erupted through continental crust, which raises the possibility of crustal contamination and modification of primary magma chemistry during their ascent to the surface. Any such contamination effects must be eliminated before the primary mantle source characteristics can be evaluated, which is accomplished here using various interelement ratios of the Pali Aike and Morro Chico lavas. Although conventional indicators such as Ba/La and La/Ta are known to be easily fractionated by some igneous processes, the Ce/Pb and Nb/U ratios of the MORB–OIB field show virtually constant values ($Ce/Pb = 25 \pm 5$ and $Nb/U = 47 \pm 7$, Hofmann *et al.* 1986) and are higher than the value for average continental crust or arc volcanic rocks (Taylor & McLennan

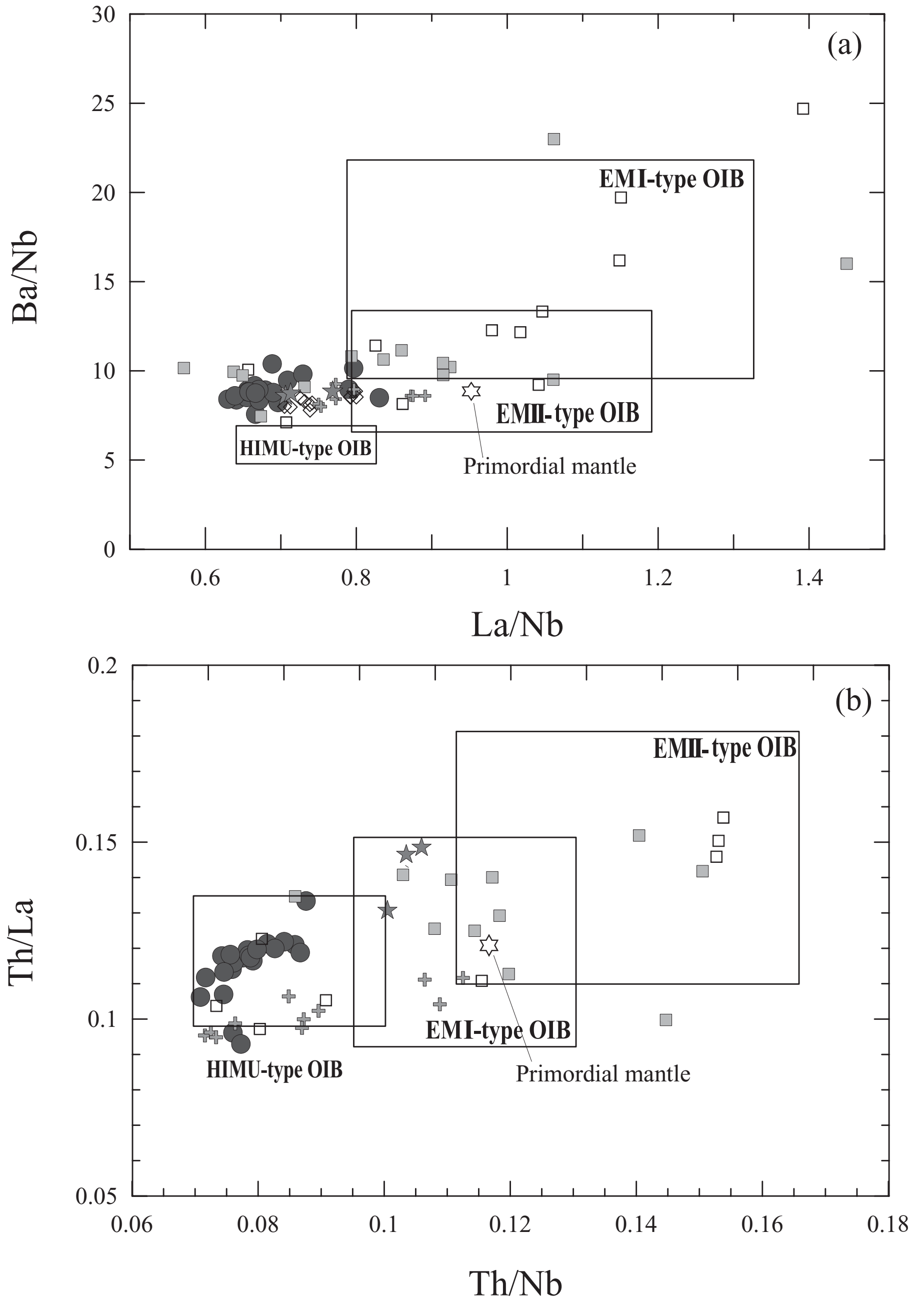

Fig. 5 Plots of (a) Ba/Nb *vs* La/Nb and (b) Th/La *vs* Th/Nb for the Pali Aike and Morro Chico samples illustrating overall lower LILE/HFSE and LREE/HFSE ratios compared to some other southern Patagonian slab window lavas, and similarity with HIMU–OIB. Fields for the primordial mantle, HIMU, EMI, and EMII are from Weaver (1991). Symbols and data sources for the southern Patagonian slab window lavas are the same as those in Figure 3.

1985). These elements are not fractionated relative to one another during partial melting or fractional crystallization, and thus their ratios reflect those of source regions (Hofmann *et al.* 1986). The ratios of Ce/Pb and Nb/U for the majority of Pali Aike samples are within the range of oceanic basalts (Fig. 8). In contrast, the ratios of these elements in the analyzed Morro Chico samples (Ce/Pb = 15.0–16.7, Nb/U = 32.6–34.7) plot slightly lower than do those of oceanic basalts. The slightly lower Ce/Pb and Nb/U ratios of the Morro Chico samples, along with the occurrence of quartz xenocrysts in some sections, may suggest the presence of crustal assimilation processes at some stage during the magma ascent, but their depleted $^{87}Sr/^{86}Sr$ and $^{143}Nd/^{144}Nd$ isotopic signatures relative to the Southern Patagonian slab window lavas (Fig. 6) indicate only a minor role of crustal assimilation in the petrogenesis of the Morro Chico lavas. The Pali Aike and Morro Chico lavas also have relatively high $(Nb/La)_{PM}$ (Pali Aike ~1.4 and Morro Chico ~1.3) and low $(Th/Nb)_{PM}$ ratios (Pali Aike ~0.67 and Morro Chico ~0.87) and do not exhibit Nb and Ta deple-

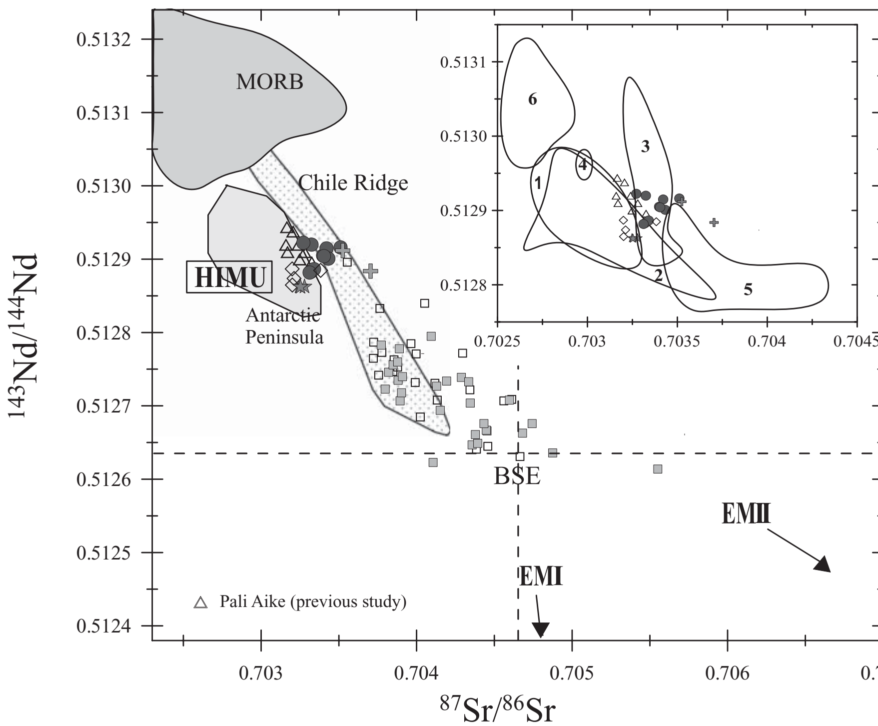

Fig. 6 Sr and Nd isotopic compositions of Pali Aike and Morro Chico samples. Some other southern Patagonian slab window lavas show relatively enriched OIB-like signatures compared to the HIMU-like signatures of the Pali Aike and Morro Chico samples, which display depleted. Slab window lavas from the Antarctic Peninsula show compositions similar to those of the Pali Aike and Morro Chico samples. Data sources: Pali Aike, Stern *et al.* (1990) and D'Orazio *et al.* (2000); Estancia Glencross area, D'Orazio *et al.* (2001); main plateau lavas and post-plateau lavas, Gorring and Kay (2001) and Gorring *et al.* (2003); and Camusu Aike, D'Orazio *et al.* (2005). Mantle components (EMI, EMII, and HIMU) are from Zindler and Hart (1986). MORB field and Chile ridge lavas (segments 1, 2, and 4) are compiled from Hofmann (1997) and Sturm *et al.* (1999). Also plotted are fields in the inset for (1) slab window lavas from the Antarctic Peninsula, Hole *et al.* (1993); (2) alkali basalts from West Antarctica, Hart *et al.* (1997) and Panter *et al.* (2000); and (3, 4, 5, and 6) mantle xenoliths from the Pali Aike volcanic field, Stern *et al.* (1999). Symbols are the same as those in Figure 3.

tions. This confirms that contributions of crustal and/or lithospheric mantle material were not significant in the generation of the Pali Aike and Morro Chico magmas. Finally, the ubiquitous presence of mantle xenoliths in the Pali Aike volcanic field suggests that magma ascended rapidly to the surface without significant interaction with crystalline wall rocks. This indicates that the chemistry of the Pali Aike and Morro Chico lavas can be used to constrain the characteristics of the original mantle sources.

MELTING PROCESSES: REE MODELING

Contributions from crustal and/or lithospheric material to the petrogenesis of the Pali Aike and Morro Chico lavas have been shown to be insignificant, and thus their geochemical variations probably resulted primarily from the partial melting of mantle sources at different depths. The degree of partial melting in basalt genesis can be estimated using highly incompatible trace element ratios, which remain constant during fractional crystallization, but which vary during partial melting. The Nb/Y ratio is one such index because Nb and Y express a range of incompatibilities in the mantle source materials and have been found to be least affected by metasomatic processes (e.g. Rogers *et al.* 1992; Beard *et al.* 1998). FeO and SiO_2 contents may also reflect the degree of partial melting and/or melting depths (Klein & Langmuir 1987; Langmuir *et al.* 1992; Nicholson & Latin 1992). Low-degree melts are commonly generated at greater depths and have higher total Fe and lower silica contents (Langmuir *et al.* 1992). The higher FeO and lower SiO_2 contents, and the higher Nb/Y ratios of the Pali Aike samples compared to those of the Morro Chico lavas (Fig. 9) indicate that the Pali Aike lava was generated by lower degrees of partial melting in deeper part of the mantle.

Other constraints for the degree of partial melting and residual mineralogy in the formation of the Pali Aike and Morro Chico magmas can be

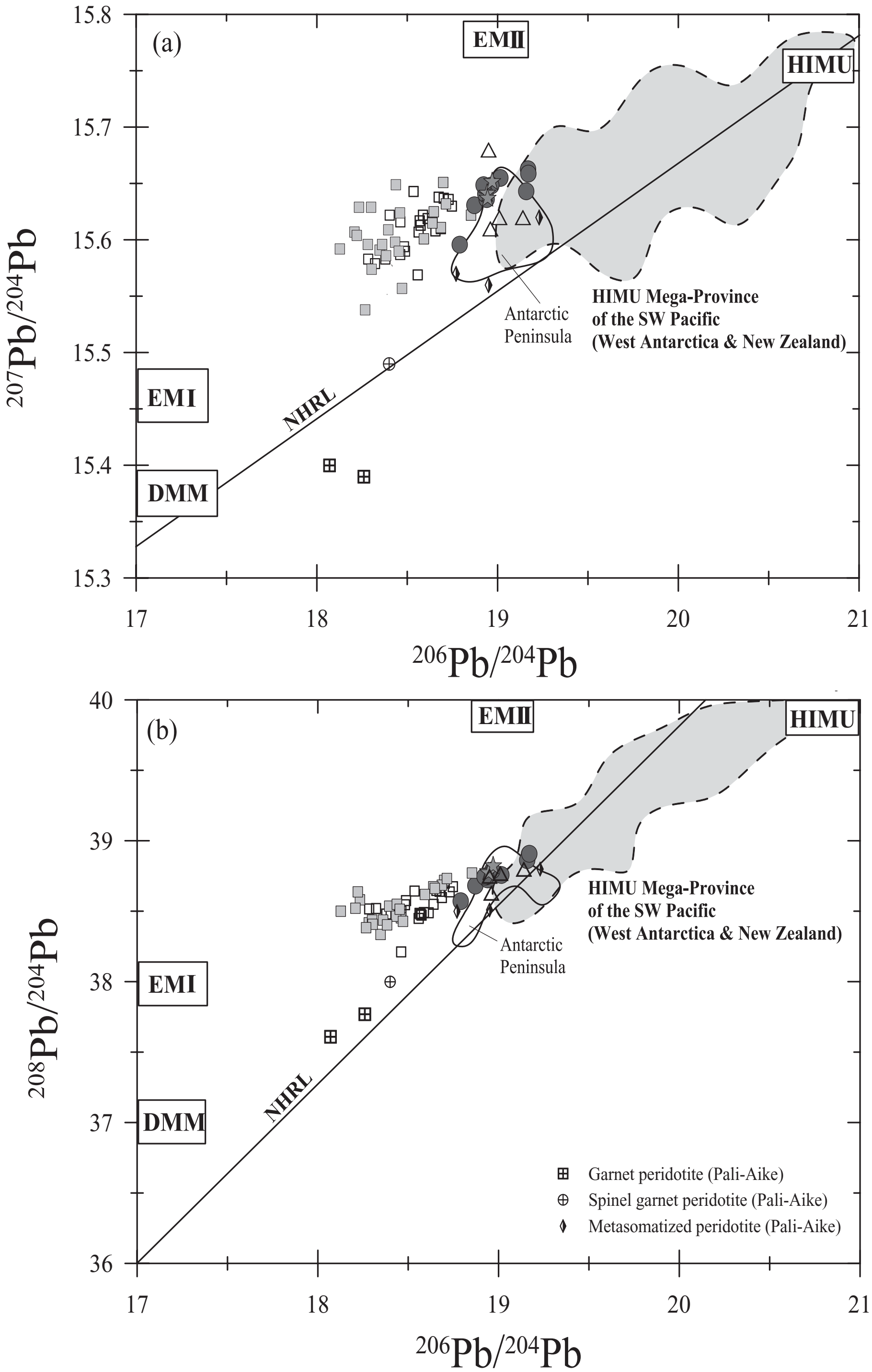

Fig. 7 Plots of (a) $^{207}Pb/^{204}Pb$ and (b) $^{208}Pb/^{204}Pb$ *vs* $^{206}Pb/^{204}Pb$ for the Pali Aike and Morro Chico samples compared to previously published data for southern Patagonian plateau basalts and mantle xenoliths from the Pali Aike. Symbols, abbreviations, and data sources are the same as in Figure 6. Field labeled 'HIMU Mega-Province of the SW Pacific' represents isotopic compositions of alkali basalts from West Antarctica and New Zealand that show HIMU-like OIB signatures (Hart *et al.* 1997; Panter *et al.* 2000; Hoernle *et al.* 2006; Panter *et al.* 2006; Timm *et al.* 2009 and McCoy-West *et al.* 2010). The data field for slab window lavas from the Antarctic Peninsula is from Hole *et al.*, 1993. Symbols are the same as those in Figure 3.

obtained considering the REE systematics of lavas. Strong fractionation between light and heavy REE of the Pali Aike ($(La/Yb)_N = 11.2$–21) and Morro Chico lavas ($(La/Yb)_N = 9.7$–10.6) point to residual garnet in the source because it is almost the only phase in mantle mineralogy capable of fractionating these two sets of elements (Rollinson 1993).

To evaluate the degree of partial melting in the mantle for the Pali Aike and Morro Chico lavas, we performed REE modeling on the garnet lherzolite source using the classic, non-modal batch melting equations of Shaw (1970), with the K_D values from McKenzie and O'Nions (1991). Potential mantle sources tested include a primitive mantle (Sun & McDonough 1989) and an enriched asthenospheric

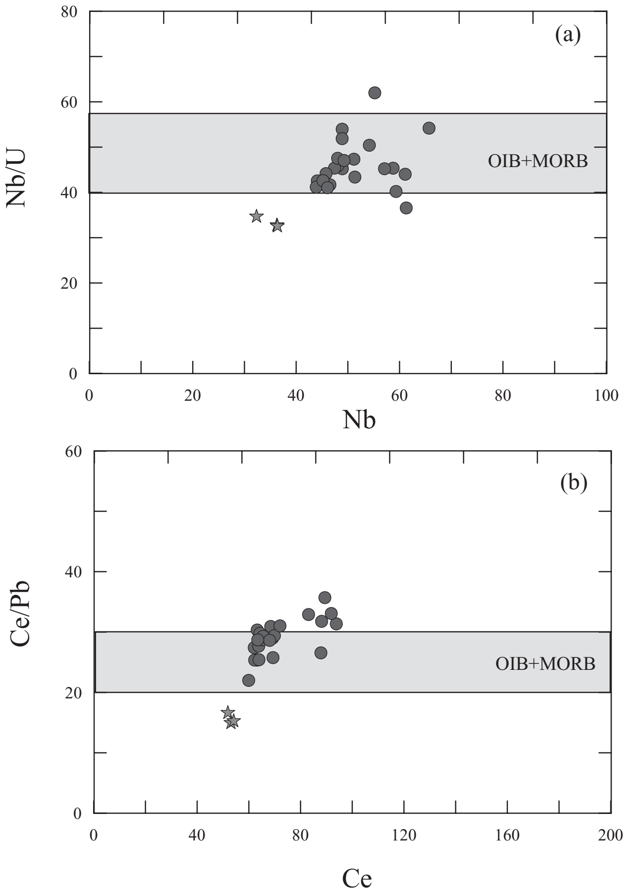

Fig. 8 Plots of (a) Nb/U *vs* Nb and (b) Ce/Pb *vs* Ce for the Pali Aike and Morro Chico samples. Pali Aike and Morro Chico lavas plot near or within fields for oceanic basalts (OIB and MORB). The average values of Nb/U and Ce/Pb for OIB and MORB are after Hofmann *et al.* (1986). Symbols are the same as those in Figure 3.

mantle source (Tang *et al.* 2006). They are assumed as starting sources to explain the OIB-like enriched geochemical features of the Pali Aike and Morro Chico lavas. The source and melt mineralogy used in modeling are similar to those used in other partial melting calculations (e.g. Witt-Eickschen & Kramm 1998; Tang *et al.* 2006). The calculated melting curves are shown in Figure 10. All mantle phases are assumed to remain as residue in the partially melted lherzolite because none is completely removed at degrees of partial melting from 0.5 to 10%. The REE chemistry of the Pali Aike and Morro Chico samples both can be successfully modeled using the enriched mantle concentrations of Tang *et al.* (2006). The fits between concentrations of REEs calculated from the enriched source and those observed in the studied samples are good and appear to reproduce the Pali Aike and Morro Chico basalts by degrees of partial melting between about 1% and about 2.7%.

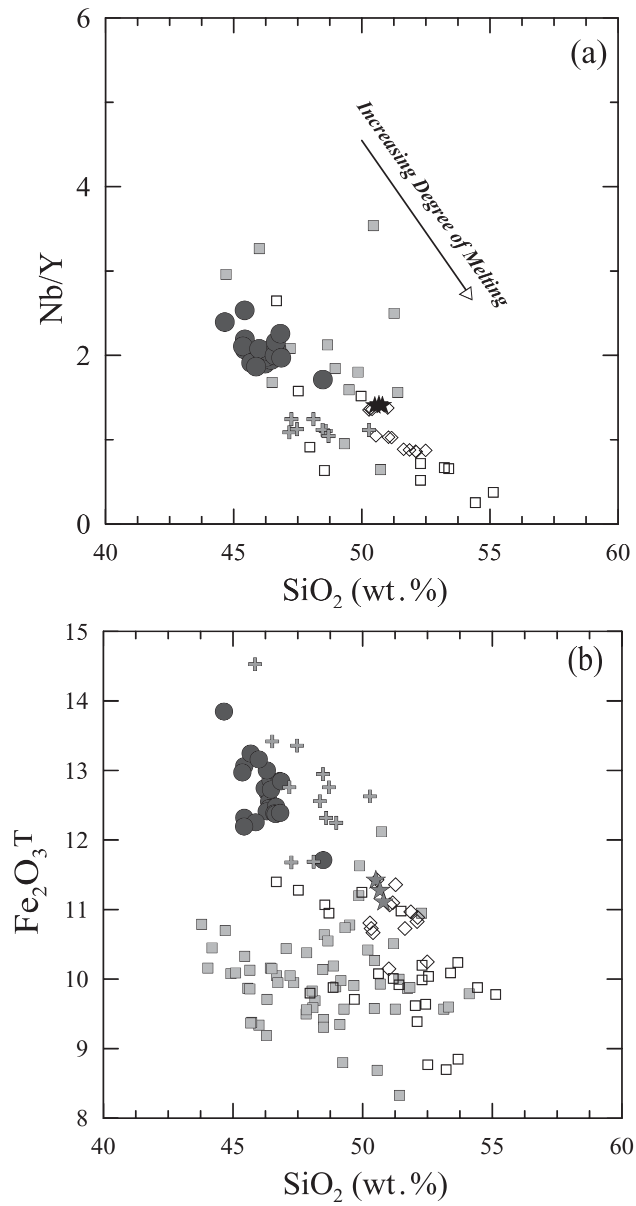

Fig. 9 Plots of (a) Nb/Y and (b) $Fe_2O_3^T$ *vs* SiO_2. Symbols and data sources are the same as those in Figure 3.

Partial melting of between 1.0% and 2.0% of an enriched mantle source containing 7 wt.% garnet could account, respectively, for the range of high and low REE contents in the Pali Aike samples (Fig. 10b). REE patterns of the Morro Chico samples are reproduced by about 2.6–2.7% melting of the same enriched mantle source (Fig. 10b). This indicates that melt generation of the Pali Aike and Morro Chico lavas occurred in the garnet–peridotite stability zone (i.e. >80 km depth) by melting of 1 to 2.7%.

In contrast, the major element chemistry (high SiO_2 and low FeO contents) of the Morro Chico

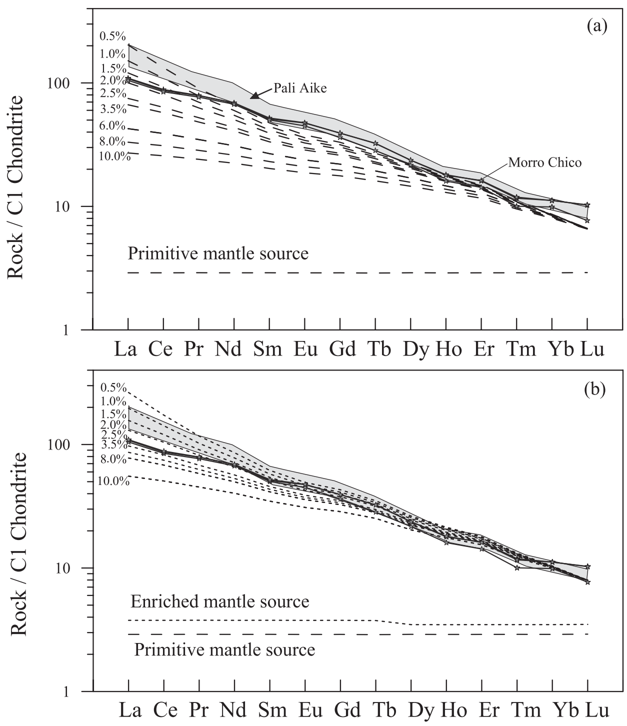

Fig. 10 Chondrite (CI)-normalized REE patterns for the Pali Aike and Morro Chico samples, with calculated model compositions. Modeling was performed for a garnet–lherzolite mantle mineralogy with source compositions of (a) a primitive mantle (Sun & McDonough 1989), and (b) an enriched asthenospheric mantle (Tang *et al.* 2006). A constant source and melt mode of $ol_{0.60} + opx_{0.18} + cpx_{0.15} + gt_{0.07}$ and $ol_{0.25} + opx_{0.20} + cpx_{0.40} + gt_{0.15}$ are used for all model calculations.

lavas is indicative of their segregation from low-pressure mantle (<15 kb, ~50 km) (Hirose & Kushiro 1993). This apparent contradiction between the major element and REE chemistry of the Morro Chico lavas is considered to have resulted from crustal assimilation processes in the generation of the Morro Chico magma. D'Orazio *et al.* (2001) suggested that interaction of mantle melts with depleted peridotites during their slow ascent may lead to an increase in the SiO_2, and to a dilution, without significant fractionation of the REE in the magma. This slow uprise of melts seems to be related to the dominant compressive tectonic regime of this region (Kraemer 1998), and in turn gives an indirect explanation for emplacement of a comparatively small volume of the Morro Chico lavas.

REGIONAL VARIATIONS AND MANTLE SOURCES

Geochemical variations in the southern Patagonian lavas can be discussed in the framework of Cenozoic regional geodynamic evolution, which constrains the relative contributions of different geochemical components such as depleted or enriched sub-slab asthenosphere, enriched continental lithospheric mantle, and subducted material. The initial ridge collisions with the Chile Trench started at 15–14 Ma in Tierra del Fuego (55°S), the southern tip of Patagonia (Cande & Leslie 1986; Lothian 1995). The next two segments, bounded by the Decolacion, Madre de Dios, and Esmeralda fracture zones, collided at 14–13 Ma and 12 Ma, after which the Chile Trench Junction migrated northward through a series of collisions involving three shorter ridge segments that collided at 6 Ma, 3 Ma, and 0.1 Ma (Fig. 1) (Lothian 1995). The Morro Chico and Pali Aike lavas of the study area erupted at 8 Ma and 3.5 Ma, 6–10 m.y. after the ridge-trench collision (D'Orazio *et al.* 2000, 2001). In contrast, extensive subalkaline basalts (main plateau lavas) of southern Patagonia north of the study area erupted at the same time as the ridge collision (12 Ma, Forsythe & Nelson 1985; Cande & Leslie 1986; Forsythe *et al.* 1986).

The geodynamic conditions of each of these regions are thought to reflect differences in the chemical and physical characteristics of the sub-slab asthenospheric mantle involved in magma genesis. The majority of southern Patagonian lavas are characterized by an incompatible element distribution pattern that is typical of within-plate basalts (Fig. 4). The Pali Aike and Morro Chico lavas exposed in southernmost South America have characteristics that are similar to those of end-member HIMU basalts (e.g. low Rb/La, Ba/La, and Ba/Nb), which distinguishes them from most of the main and post-plateau lavas in southern Patagonia (Gorring & Kay 2001).

The Southern Patagonian lavas exhibit variations in Ba/Nb, La/Nb, Th/La, and Th/Nb ratios, which are considered to be representative incompatible trace element ratios that characterize specific mantle sources (Fig. 5). The main and post plateau lavas display high Ba/Nb, La/Nb, Th/La, and Th/Nb ratios, plotting in the EMI- and EMII-type OIB fields. The Ba/Nb and La/Nb ratios of the main and post-plateau lavas show a strongly linear trend from low Ba/Nb and La/Nb ratios toward high Ba/Nb and La/Nb ratios, reflecting variable degrees of mixing between depleted HIMU-like sources (low Ba/Nb and La/Nb) and more enriched mantle sources (high Ba/Nb and La/Nb). In contrast, the Camusu Aike lavas, which erupted at slightly higher latitude (~51°S) than the study area, show more limited compositional ranges, plotting in the HIMU–OIB field, and have lower Ba/Nb, La/Nb, Th/La, and Th/Nb ratios than do the main and post-plateau lavas, which erupted north of the study region (46.5°S–49.5°S).

Systematic spatial variations are also evident in Sr, Nd, and Pb isotopic compositions. In spite of the different eruption ages of the main and post plateau volcanic lavas, these lavas have similar Sr–Nd–Pb isotopic compositional ranges. Their compositions extend into somewhat more radiogenic $^{87}Sr/^{86}Sr$, and less radiogenic $^{143}Nd/^{144}Nd$ and $^{206}Pb/^{204}Pb$ fields, indicating a dominant contribution from an EMI-like mantle component (Fig. 11). In contrast, the isotopic compositions of the Pali Aike and Morro Chico samples form fields that are distinct from those of the main and post-plateau lavas, having compositions similar to those of slab window-related alkali lavas from the Antarctic Peninsula and partly overlapping with low $^{206}Pb/^{204}Pb$ ratio basalts from West Antarctica and New Zealand, and tending toward the HIMU mantle end-member composition. The volcanic fields of the Antarctic Peninsula, West Antarctica, and New Zealand were adjacent to one another prior to the breakup of Gondwana and are grouped as a 'magmatic HIMU mega-province' in the southwestern Pacific (e.g. Hart *et al.* 1997; Panter *et al.* 2006; McCoy-West *et al.* 2010). The southernmost tip of South America, where the Pali Aike and Morro Chico lavas are exposed, is geographically close to the Antarctic Peninsula, which suggests the presence of the common HIMU mantle component beneath both southernmost Patagonia and the HIMU mega-province of the southwestern Pacific.

The most southern Patagonian plateau lavas have OIB-like trace element and isotopic affinities and show little evidence for significant contamination by continental crustal components. The common occurrence of mantle xenoliths in the basaltic lavas indicates rapid magma ascent with little time to interact with the crust. Together, these lines of evidence argue for uncontaminated mantle source signatures. Generally, two mantle components can be considered as possible source materials for continental basaltic magma generation: continental lithospheric mantle and shallow, upwelling asthenospheric mantle.

Geochemical studies (Gorring *et al.* 2003; Bruni *et al.* 2008) have proposed that EMI-like higher $^{87}Sr/^{86}Sr$ and lower $^{143}Nd/^{144}Nd$ and $^{206}Pb/^{204}Pb$ isotopic features observed in most of the main and post plateau lavas in the region between 46.5°S and 49.5°S originated from the contribution of sub-

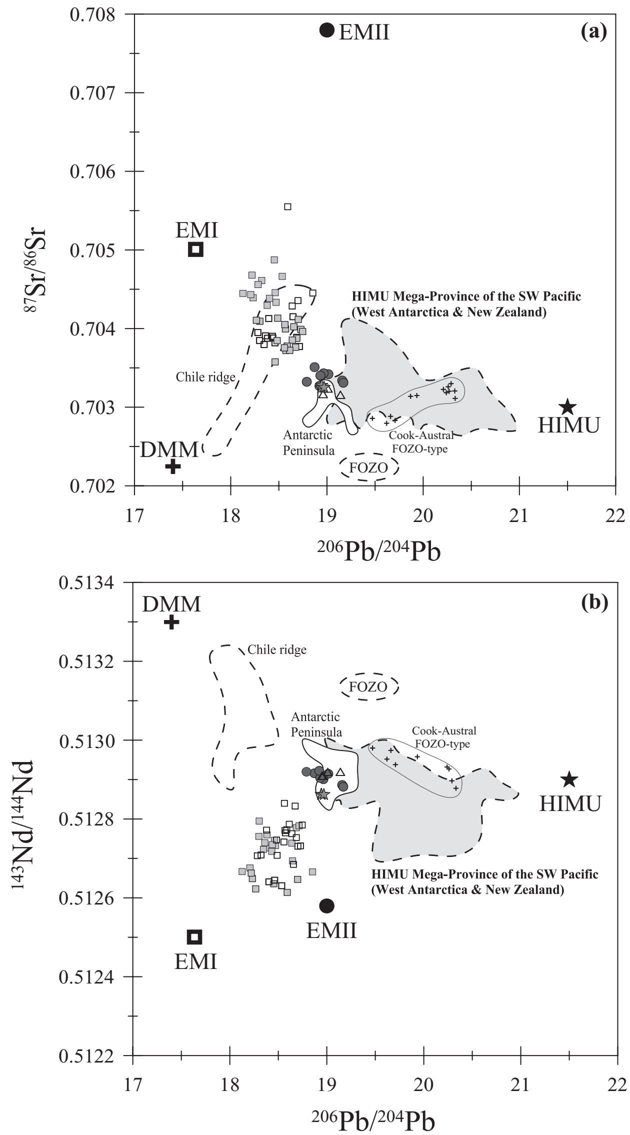

Fig. 11 Plots of (a) $^{87}Sr/^{86}Sr$ and (b) $^{143}Nd/^{144}Nd$ *vs* $^{206}Pb/^{204}Pb$ for the southern Patagonian plateau lavas. Compositions of volcanic rocks from the HIMU magmatic mega-province of the SW Pacific and slab window lavas from the Antarctic Peninsula are plotted together for comparison (see captions for Figs 6,7 for data sources and symbols). Mantle components (DM, EMI, EMII, and HIMU) and the field of Chile ridge lavas (segments 2 and 4) are compiled from Zindler and Hart (1986) and Sturm *et al.* (1999).

continental lithospheric mantle (SCLM) melts. However, several lines of evidence from recent mantle xenolith studies (e.g. Stern *et al.* 1999; Gorring & Kay 2000; Kilian & Stern 2002; Schilling *et al.* 2008) do not support continental lithospheric mantle as a potential isotopically enriched reservoir for the southern Patagonian main and post-plateau lavas.

EMI-type mantle components with relatively low $^{143}Nd/^{144}Nd$ and $^{206}Pb/^{204}Pb$ ratios are attributed to time-integrated low U/Pb and Sm/Nd ratios in the source. To develop isotopically enriched EMI-like reservoirs, sufficient time (>1 b.y.) is required for interaction with metasomatic agents such as ancient silicate melt and/or $CO_2 \pm H_2O$-rich fluids or carbonatite melts (e.g. Zindler & Hart 1986). However, the relatively young lithospheric mantle beneath southern Patagonia (Schilling *et al.* 2008) and recent (<25 Ma) metasomatic events recognized by mantle xenolith studies (Gorring & Kay 2000; Laurora *et al.* 2001; Kilian & Stern 2002; Bjerg *et al.* 2005; Conceicão *et al.* 2005; Wang *et al.* 2008) do not support the existence of EMI-like mantle components in the SCLM of southern Patagonia. Instead, local EMI-like mantle domains may exist in the southern Patagonian asthenospheric mantle. Isotopic data for mantle xenoliths from southern Patagonia show depleted Sr–Nd isotopic compositions and Pb isotope ratios that are similar to Pacific MORB (Stern *et al.* 1999; Gorring & Kay 2000) (Figs 6,7). Isotopically enriched EMI-like lithospheric mantle peridotites have not yet been identified in mantle xenoliths from the area. However, the occurrence of isotopically enriched domains in lithospheric mantle under southern Patagonia, which were not sampled by mantle xenoliths, cannot be totally excluded.

Overall, geochemical data for the Pali Aike and Morro Chico lavas, including their spatiotemporal distribution and petrological and geochemical characteristics, suggest their derivation from deep and relatively depleted asthenospheric mantle. Similarly, we propose that the OIB-like chemical and isotopic systematics of the Neogene alkali lavas that erupted in southern Patagonia originated in the asthenospheric mantle.

HIMU SIGNATURES IN THE PALI AIKE LAVAS

Large Miocene to recent alkaline volcanic belts that extend from the southernmost tip of South America via the Antarctic Peninsula and West Antarctica to New Zealand, were former neighbors in the supercontinent Gondwana (e.g. Rapalini 2005; Pankhurst *et al.* 2006) and share geochemical and isotopic features. The existence of a long-lived and widespread HIMU mantle source region (HIMU magmatic mega-province) in the southwestern Pacific, extending from West Antarctica and the sub-Antarctic Islands to New Zealand, has been suggested in a number of studies of intraplate basalts that were erupted sporadically over the last 100 m.y. in these regions (e.g. Panter *et al.* 2006; Timm *et al.* 2009, 2010; McCoy-West *et al.* 2010). Geochemical similarities shared by widespread alkaline rocks of the Pali Aike and Morro Chico and the HIMU magmatic mega-province in the southwestern Pacific suggest that these intraplate magmas were derived from mantle sources with a common history, and that these sources were probably located in the lithospheric mantle.

The petrogenesis of the continental intraplate basalts of the HIMU magmatic mega-province in the southwestern Pacific has been a subject of intense debate (e.g. Ferrar & Dixon 1984; Coombs *et al.* 1986; Weaver *et al.* 1994; Finn *et al.* 2005; Hoernle *et al.* 2006; Panter *et al.* 2006; Sprung *et al.* 2007; Timm *et al.* 2009, 2010). The classic models for explaining this volcanism can be divided into two groups: low-degree melting of metasomatized lithospheric mantle including a HIMU-like mantle component by earlier subduction- and plume-related processes (Finn *et al.* 2005; Panter *et al.* 2006; Sprung *et al.* 2007), or removal (detachment) of metasomatized lithospheric mantle, resulting in asthenospheric upwelling and melting (Hoernle *et al.* 2006; Mortimer *et al.* 2006; Timm *et al.* 2009).

As noted above, the geochemical and isotopic compositions of the Pali Aike and Morro Chico lavas are distinct from those of the majority of southern Patagonian plateau basalts (Figs 4,6,7). The Pali Aike and Morro Chico lavas have the most depleted Sr–Nd isotopic compositions of the Neogene Patagonian plateau lavas in southernmost South America (D'Orazio *et al.* 2000, 2001). The Pb isotopic compositions of the Pali Aike and Morro Chico volcanic rocks fall between end-member HIMU from St Helena and the HIMU magmatic mega-province of the southwestern Pacific, and Chilean MORB (Fig. 11).

Such compositions could reflect relatively young HIMU recycling ages for the oceanic lithosphere (e.g. Thirlwall 1997; Hoernle *et al.* 2006) or mixing between HIMU and DMM sources.

Alternatively, the isotopic compositions of the Pali Aike and Morro Chico lavas are comparable to Sr, Nd, and Pb isotope compositions of the Focus Zone (FOZO) component (Hart *et al.* 1992; Hauri *et al.* 1994; Stracke *et al.* 2005). It has been proposed that the FOZO component represents a common and ubiquitous component present in the lower mantle or MORB source mantle (Hart *et al.* 1992; Hauri *et al.* 1994; Stracke *et al.* 2005), and that it can be produced continuously by recycling of oceanic crust (Stracke *et al.* 2005). The time-integrated evolution of U/Pb versus Rb/Sr or Sm/Nd ratios of the FOZO by definition (Stracke *et al.* 2005) is known to be positively or negatively coupled. Consequently, the isotopic variations in FOZO-type basalts usually show positive or negative correlations in $^{206}Pb/^{204}Pb$ versus $^{87}Sr/^{86}Sr$ or $^{143}Nd/^{144}Nd$ diagrams (Fig. 11), overlapping and extending the trend of MORB (Hauri *et al.* 1994; Workman *et al.* 2004; Stracke *et al.* 2005). However, the Pali Aike, Morro Chico, HIMU magmatic mega-province of the southwest Pacific and Antarctic Peninsula data display no coherent correlation between Sr and Nd isotope ratios and $^{206}Pb/^{204}Pb$ ratios, in contrast to basalts derived from the FOZO (Fig. 11). Moreover, the Pali Aike and Morro Chico lavas are similar in geochemistry to that of the end-member HIMU basalts (Figs 4,5). These several lines of evidence suggest the contribution of HIMU-like mantle material to the generation of the magmas not from FOZO-like sources. Although the Pb isotopic compositions of the Pali Aike and Morro Chico lavas are generally less radiogenic than those of the end-member HIMU samples and the majority of HIMU magmatic mega-province of the southwestern Pacific, these geochemical differences could reflect different proportions of contributions of HIMU-type mantle to magma generation. In summary, the trace element chemistry and Sr–Nd–Pb isotopic compositions of the Pali Aike and Morro Chico lavas provide unequivocal evidence for the presence of HIMU-type asthenospheric mantle beneath southernmost Patagonia.

The Pali Aike and Morro Chico lavas are geographically situated near a destructive plate margin characterized by a long history of subduction. Supra-slab mantle under this kind of geodynamic setting seems to have been contaminated by slab-derived fluids and/or melts, and probably also modified by the extraction of calc-alkaline melts. Thus, explanation of the pristine OIB-like geochemical characteristics of the Pali Aike and Morro Chico lavas requires a mechanism to replace the slab-modified mantle with an unmodified mantle. Previous interpretations proposed that the lavas were derived by decompression melting of a depleted sub-slab asthenospheric source that originated through an opening slab window (e.g. D'Orazio *et al.* 2000; Gorring *et al.* 2003; Espinoza *et al.* 2005). The HIMU-like geochemical signatures of the Pali Aike and Morro Chico lavas have never been discussed in detail.

Recent studies of southern Patagonian mantle xenoliths provide information relevant to the formation and later modification of the SCLM of the southern Patagonian terrain (Kempton *et al.*, 1999a,b; Stern *et al.* 1999; Gorring & Kay 2000; Laurora *et al.* 2001; Kilian & Stern 2002; Bjerg *et al.* 2005; Conceicão *et al.* 2005; Wang *et al.* 2008; Schilling *et al.* 2008). On the basis of Re–Os isotopic data for mantle xenoliths from mid-Paleogene (Eocene) to recent alkaline basalts in southern South America, Schilling *et al.* (2008) suggested that most of the basement and SCLM below the southern Patagonian area is not Archean or early Proterozoic, but is instead of a relatively young Phanerozoic age and formed recently from a heterogeneous, convecting mantle. This provides indirect evidence for the absence of old (>1–2 Ga) recycled oceanic crust, which is considered to be the most plausible explanation for the trace element and isotope systematics in HIMU end-member basalts derived from lithospheric mantle (White 1985; Zindler & Hart 1986; Stracke *et al.* 2003; Willbold & Stracke 2006). MORB-like Sr–Nd–Pb, Os, and O isotopic compositions from the Pali Aike mantle xenoliths (Stern *et al.* 1999; Schilling *et al.* 2008) provide no evidence for the existence of a HIMU domain in the lithospheric mantle beneath these regions. In addition, local melting of cold, dense lithospheric mantle due to heat conduction in the asthenosphere would be insufficient to generate the extensive partial melting required to account for the large volumes of plateau basalt in southern Patagonia.

Delamination or detachment (removal) of dense lower lithosphere has been proposed to explain a number of intraplate basalts (e.g. Knapp *et al.* 2005; Korenaga 2005; Valera *et al.* 2008). According to these models, detachment of dense lithosphere containing eclogite, garnet pyroxenite, and Fe-rich garnet–lherzolite beneath the continental plateau region could drive convective currents, which could cause detached mantle to upwell locally and melt. Timm *et al.* (2010) suggested that the extensive Cenozoic intraplate volcanism of Zealandia, New Zealand micro-continent (e.g. Hoernle *et al.* 2006; Timm *et al.* 2009), can be explained by local lithospheric removal and subsequent decompression melting of upwelling heterogeneous asthenosphere containing detached lithosphere. Eclogite or pyroxenite and/or detached volatile-enriched lithospheric components incorporated into the heterogeneous asthenosphere are believed to contribute to the generation of the HIMU-like isotopic compositions (Hoernle *et al.* 2006; Timm *et al.* 2009).

In a similar way, the generation of Pali Aike and Morro Chico magmas can be explained by decompression melting of asthenospheric mantle that contained detached lithosphere with a HIMU-type signature. Fragments of detached lithosphere with a HIMU-type composition, in the form of eclogite and/or pyroxenite, may be present in the upper asthenosphere beneath southernmost Patagonia. The HIMU-like mantle signature may have been produced from subduction-related melts along the Gondwana margin throughout the Mesozoic and is probably related to the common lithospheric source of the HIMU mega-province in the southwestern Pacific. Here, we conclude that the EMI- and HIMU-like mantle signatures of southern Patagonian plateau basalts were derived from asthenospheric mantle that upwelled through widening slab windows, and that a major discontinuity in the isotopic composition of the asthenospheric mantle may exist near 50°S latitude.

CONCLUSIONS

1. The Pali Aike and Morro Chico lavas are alkaline and subalkaline and relatively primitive (Pali Aike 9.5–13.7 wt.% MgO; Morro Chico 7.6–8.8 wt.% MgO) mafic volcanics that have OIB-like trace element compositions (Nb/U = 32.59–62.02; La/Ta = 10.05–14.49; Th/Nb = 0.07–0.11).
2. The Pali Aike and Morro Chico lavas have relatively LREE-enriched patterns ($La_N/Yb_N = 11.2–21.0$ for the Pali Aike lavas; $La_N/Yb_N = 9.7–10.6$ for the Morro Chico lavas), suggesting their derivation from a small degree of partial melting of OIB-like asthenospheric mantle. According to the REE melting calculation, they may have been produced by very small degrees of non-modal batch melting (1.0–2.0% for Pali Aike lavas and about 2.6–2.7% for Morro Chico lavas) from a garnet lherzolite mantle source.
3. The large variations in the geochemical and Sr–Nd–Pb isotopic compositions of the southern Patagonian plateau basalts are related to latitude. Geochemical and isotopic characteristics of the Pali Aike and Morro Chico lavas are broadly similar to those of Cenozoic HIMU basalts from the Antarctica Peninsula, West Antarctica, and New Zealand. In contrast, the geochemical characteristics of most of the other southern Patagonian basalts (between 46.5° and 49.5°S) indicate a dominant contribution from an EMI-like mantle component.
4. The Pali Aike and Morro Chico volcanism can be explained by detachment of lithospheric mantle with a HIMU-type signature and subsequent decompression melting of heterogeneous asthenospheric mantle that upwelled through a widening slab window. The heterogeneous asthenospheric mantle is thought to consist of eclogite or pyroxenite domains with HIMU-like mantle signatures within a depleted (MORB-type) peridotitic matrix. The HIMU-like mantle signatures are thought to have been produced from subduction-related melts along the Gondwanan margin throughout the Mesozoic and are probably related to the lithospheric source of the HIMU mega-province in the southwestern Pacific.

ACKNOWLEDGEMENTS

We thank SH Choi, HC Kang, and WH Choe for their assistance with field work in 2009–2010 and KJ Kim for assistance with analytical work. We gratefully acknowledge the thorough and helpful reviews by Romain Meyer and Suzanne M. Kay and handling of the manuscript by Associate Editor Robert Stern, which significantly improved the quality of this paper.

This study was supported by KOPRI projects (PE12060; Korea Curation of Antarctic Meteorites and Evolutionary Materials) and partly funded by the National Foundation of Korea (2009-0470-2-2).

REFERENCES

Beard A. D., Downes H., Hegner E., Sablukov S. M., Vetrin V. R. & Balogh K. 1998. Mineralogy and geochemistry of Devonian ultramafic minor intrusions of the southern Kola Peninsula, Russia: Implication for the petrogenesis of kimberlites and melilitites. *Contribution to Mineralogy and Petrology* **130**, 288–303.

Bjerg E. A., Ntaflos T., Kurat G., Dobosi G. & Labadía C. H. 2005. The upper mantle beneath Patagonia, Argentina, documented by xenoliths from alkali basalts. *Journal of South American Earth Sciences* **18**, 125–45.

Bruni S., D'Orazio M., Haller M. J. *et al.* 2008. Time-evolution of magma sources in a continental back-arc setting: The Cenozoic basalts from Sierra de San Bernardo (Patagonia, Chubut, Argentina). *Geological Magazine* **145**, 741–32.

Cande S. C. & Leslie R. B. 1986. Late Cenozoic tectonics of the southern Chile trench. *Journal of Geophysical Research* **91** (B1), 471–96.

Choi S. H., Mukasa S. B., Kwon S.-T. & Andronikov A. V. 2006. Sr, Nd, Pb and Hf isotopic compositions of late Cenozoic alkalibasalts in South Korea: Evidence for mixing between the two dominant asthenospheric mantle domains beneath East Asia. *Chemical Geology* **232**, 134–51.

Cole R. B. & Basu A. R. 1995. Nd-Sr isotopic geochemistry and tectonics of ridge subduction and middle Cenozoic volcanism in western California. *Geological Society of America Bulletin* **107**, 167–79.

Conceicão R. V., Mallmann G., Koester E., Schilling M., Bertotto G. W. & Rodriguez-Vargas A. 2005. Andean subduction-related mantle xenoliths: Isotopic evidence of Sr-Nd decoupling during metasomatism. *Lithos* **82**, 273–87.

Coombs D. S., Kawachi R. A., Landis C. A., McDonough W. M. & Reay A. 1986. Cenozoic volcanism in north, east and central Otago. Cenozoic volcanism in New Zealand. *Royal Society of New Zealand Bulletin* **23**, 278–312.

Corbella H. 1999. Dataciones radimetricas en Pali Aike, Patagonia Austral. *Actas del XIV Congreso Geologico Argentino* **II**, 269–72.

D'Orazio M., Agostini S., Innocenti F., Haller M. J., Manetti P. & Mazzarini F. 2001. Slab window-related magmatism from southernmost South America: The Late Miocene mafic volcanics from the Estancia Glencross Area (~52°S, Argentina-Chile). *Lithos* **57**, 67–89.

D'Orazio M., Agostini S., Mazzarini F. *et al.* 2000. The Pali Aike Volcanic Field, Patagonia: Slab-window magmatism near the tip of South America. *Tectonophysics* **321**, 407–27.

D'Orazio M., Innocentia F., Manettib P. & Hallerc M. J. 2004. The Cenozoic back-arc magmatism of the southern extra-Andean Patagonia (44.5–52°S): A review of geochemical data and geodynamic interpretations. *Revista de la Asociación Geológica Argentina* **59**, 525–38.

D'Orazio M., Innocentia F., Manettib P., Hallerc M. J., Di Vincenzo G. & Tonarini S. 2005. The Late Pliocene mafic lavas from the Camusu Aike volcanic field (~50°S, Argentina): Evidence for geochemical variability in slab window magmatism. *Journal of South American Earth Sciences* **18**, 107–24.

De Ignacio C., Lopez I., Oyarzun R. & Márquez A. 2001. The northern Patagonia Somuncura plateau basalts: A product of slab-induced, shallow asthenospheric upwelling? *Terra Nova* **13**, 117–21.

Espinoza F., Morata D., Pelleter E. *et al.* 2005. Petrogenesis of the Eocene and Mio-Pliocene alkaline basaltic magmatism in Meseta Chile Chico, southern Patagonia, Chile: Evidence for the participation of two slab windows. *Lithos* **82**, 315–43.

Ferrar E. & Dixon J. M. 1984. Overriding of the Indian-Antarctic ridge: Origin of Emerald Basin and migration of late Cenozoic volcanism in southern New Zealand and Campbell Plateau. *Tectonophysics* **104**, 243–56.

Finn C. A., Mueller R. D. & Panter K. S. 2005. A Cenozoic diffuse alkaline magmatic province (DAMP) in the southwest Pacific without rift or plume origin. *Geochemistry Geophysics Geosystems* **6**, Q02005.

Forsythe R. & Nelson E. 1985. Geological manifestations of ridge collision : Evidence from the Golfo de Penas-Taitao basin, southern Chile. *Tectonics* **4**, 477–95.

Forsythe R. D., Nelson E. P., Carr M. J. *et al.* 1986. Pliocene near-trench magmatism in southern Chile: A possible manifestation of ridge collision. *Geology* **14**, 23–7.

Futa K. & Stern C. R. 1988. Sr and Nd isotopic and trace element compositions of Quaternary volcanic centers of the southern Andes. *Earth and Planetary Science Letters* 88, 253–62.

Gorring M. L. & Kay S. M. 2000. Carbonatite metasomatized peridotite xenoliths from southern Patagonia: Implications for lithospheric processes and Neogene plateau magmatism. *Contribution to Mineralogy and Petrology* **140**, 55–72.

Gorring M. L. & Kay S. M. 2001. Mantle processes and sources of Neogene slab window magmas from Southern Patagonia, Argentina. *Journal of Petrology* **42**, 1067–94.

Gorring M. L., Kay S. M., Zeitler P. K. *et al.* 1997. Neogene Patagonian plateau lavas: Continental magma associated with ridge collision at the Chile Triple Junction. *Tectonics* **16**, 1–17.

Gorring M. L., Singer B., Gowers J. & Kay S. M. 2003. Plio-Pleistocene basalts from the Meseta del Lago Buenos Aires, Argentina: Evidence for asthenosphere-lithosphere interactions during slab window magmatism. *Chemical Geology* **193**, 215–35.

Gripp A. E. & Gordon R. G. 2002. Young tracks of hotspots and current plate velocities. *Geophysical Journal International* **150**, 321–61.

Hart S. R. 1984. The dupal anomaly: A large-scale isotopic anomaly in the southern Hemisphere mantle. *Nature* **309**, 753–6.

Hart S. R., Blusztajn J. & Craddock C. 1997. Hobbs Coast Cenozoic volcanism: Implications for the West Antarctic rift system. *Chemical Geology* **139**, 223–48.

Hart S. R., Hauri E. H., Oschmann L. A. & Whitehead J. A. 1992. Mantle plumes and entrainment: Isotopic Evidence. *Science* **256**, 517–20.

Hauri E. H., Whitehead J. A. & Hart S. R. 1994. Fluid dynamic and geochemical aspects of entrainment in mantle plumes. *Journal of Geophysical Research* **99**, 24275–300.

Hickey R., Frey F. A. & Gerlach D. 1986. Multiple sources for basaltic arc rocks from the southern volcanic zone of the Andes (34°–41°S): Trace element and isotopic evidence for contributions from subducted oceanic crust, mantle, and continental crust. *Journal of Geophysical Research* **91**, 5963–83.

Hirose K. & Kushiro I. 1993. Partial melting of dry peridotites at high pressures: Determination of compositions of melts segregated from peridotite using aggregates of diamond. *Earth and Planetary Science Letters* **114**, 477–89.

Hoernle K., White J. D. L., Bogaard P. V. D. *et al.* 2006. Cenozoic intraplate volcanism on New Zealand: Upwelling induced by lithospheric removal. *Earth and Planetary Science Letters* **248**, 335–52.

Hofmann A. W. 1997. Mantle geochemistry: The message from oceanic volcanism. *Nature* **385**, 219–29.

Hofmann A. W., Jochum K. P., Seufert M. & White W. M. 1986. Nb and Pb in oceanic basalts: New constraints on mantle evolution. *Earth and Planetary Science Letters* **79**, 33–45.

Hole M. J., Kempton P. D. & Millar I. L. 1993. Trace-element and isotopic characteristics of small-degree melts of the asthenosphere: Evidence from the alkalic basalts of the Antarctic Peninsula. *Chemical Geology* **109**, 51–68.

Kawabata H., Hanyu T., Chang Q., Kimura J.-I. & Nichols A. R. L. & Tatsumi Y. 2011. The petrology and geochemistry of St. Helena Alkali Basalts: Evaluation of the oceanic crust-recycling model for HIMU OIB. *Journal of Petrology* **52**, 791–838.

Kay S. M., Ardolino A. A., Franchi M. & Ramos V. A. 1992. The Somuncura plateau: An Oligo-Miocene 'baby-hotspot' in extra-Andean Patagonia (40.5° to 43.5° Latitude). *Eos, Transactions, American Geophysical Union* **7**, 337.

Kay S. M., Ardolino A. A., Gorring M. L. & Ramos V. A. 2007. The Somuncura large igneous province in Patagonia: Interaction of a transient mantle thermal anomaly with a subducting slab. *Journal of Petrology* **48**, 43–77.

Kempton P. D., Hawkesworth C. J., Lopez-Escobar L. & Ware A. J. 1999b. Spinel±garnet lherzolite xenoliths from Pali Aike: Part 2. Trace element and isotopic evidence bearing on the evolution of lithospheric mantle beneath southern Patagonia. *In* Gurney J. J., Gurney J. L., Pascoe M. D. and Richardson S. H. (eds.) *Proc. 7th International Kimberlite Conference, The J.B. Dawson Volume*, pp. 415–28, *Red Rood Design*, Cape Town.

Kempton P. D., Lopez-Escobar L., Hawkesworth C. J., Pearson G. & Ware A. J. 1999a. Spinel±garnet lherzolite xenoliths from Pali Aike: Part 1. Petrography, mineral chemistry and geothermobarometry. *In* Gurney J. J., Gurney J. L., Pascoe M. D. and Richardson S. H. (eds.) *Proc. 7th International Kimberlite Conference, The J.B. Dawson Volume*, pp. 403–14, *Red Rood Design*, Cape Town.

Kilian R. & Stern C. R. 2002. Constraints on the interaction between slab melts and the mantle wedge from adakitic glass in peridotite xenoliths. *European Journal of Mineralogy* **14**, 25–36.

Kim N., Song Y.-S., Park K.-H. & Lee H.-S. 2009. SHRIMP U-Pb Zircon Ages of the Granite Gneisses from the Pyeonghae Area of the northeastern Yeongnam Massif (Sobaeksan Massif). *Journal of the Petrological Society of Korea* **18**, 31–47 (in Korean with English abstract).

Klein E. M. & Langmuir C. H. 1987. Global correlations of ocean ridge basalt chemistry with axial depth and crustal thickness. *Journal of Geophysical Research* **92**, 8089–115.

Klepeis K. A. 1994. The Magallanes and Deseado fault zones: Major segments of south American-Scotia transform plate boundary in southernmost South America, Tierra del Fuego. *Journal of Geophysical Research* **99**, 22001–14.

Knapp J. H., Knapp C. C., Raileanu V., Matenco L., Mocanu V. & Dinu C. 2005. Crustal constraints on the origin of mantle seismicity in the Vrancea zone, Romania: The case for active continental lithospheric delamination. *Tectonophysics* **410**, 311–23.

Korenaga J. 2005. Why did not the Ontong Java Plateau from subaerially? *Earth and Planetary Science Letters* **234**, 385–99.

Kraemer P. E. 1998. Structure of the Patagonian Andes: Regional balanced cross section at 50° S, Argentina. *International Geology Review* **40**, 896–915.

Langmuir C. H., Klein E. M. & Plank T. 1992. Petrological systematic of mid-ocean ridge basalts: Constraints on melt generation beneath ocean ridges. *In* Phipps Morgan, J., Blankman, D. K. and Sinton, J. M. (eds.) *Mantle Flow and Melt Generation at Mid-Ocean Ridges*, pp. 183–280, American Geophysical Union, Washington, DC.

Laurora A., Mazzucchelli M., Rivalenti G. *et al.* 2001. Metasomatism and melting in carbonated peridotite xenoliths from the mantle wedge: The Gobernador Gregores case (Southern Patagonia). *Journal of Petrology* **42**, 69–87.

Le Bas M. J., Le Maitre R. W., Streckeisen A. & Zanettin B. 1986. A chemical classification of volcanic rocks based on the total alkali-silica diagram. *Journal of Petrology* **27**, 745–50.

Lee M. J., Lee J. I., Kwon S.-T. *et al.* 2011. Sr–Nd–Pb isotopic compositions of submarine alkali basalts recovered from the South Korea Plateau, East Sea. *Geosciences Journal* **15**, 149–60.

Linares E. & Gonzalez R. R. 1990. Catálogo de edades radimetricas de la Republica Argentina, años 1957–1987. *Asociacion Geologica Argentina, Publicaciones Especiales Serie B* **19**, 628.

Liu C.-Q., Masuda A. & Xie G.-H. 1994. Major- and trace-element compositions of Cenozoic basalts in eastern China: Petrogenesis and mantle source. *Chemical Geology* **114**, 19–42.

Lothian A. 1995. *An investigation of the subduction of the Chile Ridge and Louisville Ridge using GLORIA side-scan sonar and other marine geophysical data*. PhD dissertation, University of Birmingham, Birmingham.

Luhr J. F., Aranda-Gomez J. J. & Housh T. B. 1995. San Quintín Volcanic Field, Baja California Norte, Mexico: Geology, petrology, and geochemistry. *Journal of Geophysical Research* **100**, 10353–80.

LUM C. C. L., LEEMAN W. P., FOLAND K. A., KARGEL J. A. & FITTON J. G. 1989. Isotopic variations in continental basaltic lavas as indicators of mantle heterogeneity: Examples from the western U.S. Cordillera. *Journal of Geophysical Research* **94**, 7871–84.

MCCOY-WEST A. J., BAKER J. A., FAURE K. & WYSOCZANSKI R. 2010. Petrogenesis and origins of mid-cretaceous continental intraplate volcanism in Marlborough, New Zealand: Implications for the long-lived HIMU magmatic mega-province of the SW Pacific. *Journal of Petrology* **51**, 2003–45.

MCKENZIE D. P. & O'NIONS R. K. 1991. Partial melt distribution from inversion of rare earth element concentrations. *Journal of Petrology* **32**, 1021–91.

MEGLIOLI A. 1992. *Glacial Geology and Geochronology of Southernmost Patagonia and Tierra Del Fuego, Argentina and Chile*. PhD thesis, Lehigh University, Bethelehem, PA, 216pp.

MERCER J. H. 1976. Glacial history of southernmost south America. *Quaternary Research* **6**, 125–66.

MORTIMER N., HOERNLE K., HAUFF F. *et al.* 2006. New constraints on the age and evolution of the Wishbone Ridge, southwest Pacific Cretaceous microplates, and Zealandia-West Antarctica breakup. *Geology* **34**, 185–8.

MOTOKI A., ORIHASHI Y., HALLER M. J., HOSONO T. & MIBE K. 2005. Extra-backarc magmatism of the Somuncura basaltic province, Río Negro-Chubut, Argentine Patagonia and its magmagenesis by means of dehydration of β-phase olivine. III Simpósio de Vulcanismo e Ambientes Associados, Cabo Frio, 382–92.

NICHOLSON H. & LATIN D. 1992. Olivine tholeiites from Krafla, Iceland: Evidence for variations in melt fraction within a plume. *Journal of Petrology* **33**, 1105–24.

PANKHURST R. J., LEAT P. T., SRUOGA P. *et al.* 1998. The Chon Aike province of Patagonia and related rocks in West Antarctica: A silicic large igneous province. *Journal of Volcanology and Geothermal Research* **81**, 113–36.

PANKHURST R. J., PAPELA C. W., FANNIG C. M. & MÁRQUEZ M. 2006. Gondwanide continental collision and the origin of Patagonia. *Earth-Science Reviews* **76**, 235–57.

PANTER K. S., BLUSZTAIN J., HART R. S., KYLE P. R., ESSER R. & MCINTOSH W. C. 2006. The origin of HIMU in the SW Pacific: Evidence from intraplate volcanism in Southern New Zealand and Subantarctic Islands. *Journal of Petrology* **47**, 1673–704.

PANTER K. S., HART R. S., KYLE P. R., BLUSZTAIN J. & WILCH T. 2000. Geochemistry of Late Cenozoic basalts from the Crary Mountains: Characterization of mantle sources in Marie Byrd Land, Antarctica. *Chemical Geology* **165**, 215–41.

RAMOS V. A. & KAY S. M. 1992. Southern Patagonian plateau basalts and deformation: Backarc testimony of ridge collisions. *Tectonophysics* **205**, 261–82.

RAPALINI A. E. 2005. The accretionary history of southern South America from the latest Proterozoic to the late Paleozoic: Some palaeomagnetic constraints. *In* Vaughan A. P. M., Leat P. T. and Pankhurst R. J. (eds.) *Terrane Processes at the Margins of Gondwana*. Geological Society of London, Special Publication 246, pp. 305–28.

ROGERS N. W., HAWKESWORTH C. J. & PALACZ Z. A. 1992. Phlogopite in the generation of olivine-melilitites from Namaqualand, South Africa and implications for element fractionation processes in the upper mantle. *Lithos* **28**, 347–65.

ROLLINSON H. 1993. *Using geochemical data; evaluation, presentation, interpretation*. Longman Scientific and Technical, Harlow.

ROSS P.-S., DELPIT S., HALLER M. J., NÉMETH K. & CORVELLA H. 2011. Influence of the substrate on maar-diatreme volcanoes – An example of a mixed setting from the Pali Aike volcanic field, Argentina. *Journal of Volcanology and Geothermal Research* **201**, 253–71.

SCHILLING M. E., CARLSON R. W., CONCEICÃO R. V., DANTAS C., BERTOTTO G. W. & KOESTER E. 2008. Re-Os isotope constraints on subcontinental lithospheric mantle evolution of southern South America. *Earth and Planetary Science Letters* **268**, 89–101.

SHAW D. M. 1970. Trace elements fractionation during anatexis. *Geochimica et Cosmochimica Acta* **34**, 237–43.

SINGER B. S., TON-THAT T., VINCZE T., RABASSA J., ROIG C. & BRUNSTAD K. 1997. Timescale of late Cenozoic climate change in the southern Hemisphere from $^{40}Ar/^{39}Ar$ dating of Patagonia lavas. *Terra abstracts, European Union of Geoscience* **9**, 65–6.

SPRUNG P., SCHUTH S., MÜNKER C. & HOKE L. 2007. Intraplate volcanism in New Zealand: The role of fossil plume material and variable lithospheric properties. *Contributions Mineralogy Petrology* **153**, 669–87.

STERN C. R., FREY F. A., FUTA K., ZARTMAN R. E., PENG Z. & KYSER T. K. 1990. Trace-element and Sr, Nd, Pb and O isotopic composition of Pliocene and Quaternary alkali basalt of the Patagonian plateau lavas of southernmost South America. *Contribution to Mineralogy and Petrology* **104**, 294–308.

STERN C. R. & KILIAN R. 1996. Role of the subducted slab, mantle wedge and continental crust in the generation of adakites from the Andean Austral Volcanic Zone. *Contributions to Mineralogy and Petrology* **123**, 263–81.

STERN C. R., KILLIAN R., OLKER B., HAURI E. H. & KYSER T. K. 1999. Evidence from mantle evolution for relatively thin (<100 km) continental lithosphere

below the Phanerozoic crust of southernmost south America. *Lithos* 48, 217–35.
Storey M., Rogers G., Saunders A. D. & Terrell D. J. 1989. San Quintín volcanic field, Baja California, Mexico: 'Within-plate' magmatism following ridge subduction. *Terra Nova* **1**, 195–202.
Stracke A., Bizimis M. & Salters V. J. M. 2003. Recycling oceanic crust: Quantitative constraints. *Geochemistry, Geophysics, Geosystems* **4**, 8003, doi: 10.1029/2001GC000223.
Stracke A., Hofmann A. W. & Hart S. R. 2005. FOZO, HIMU, and the rest of the mantle Zoo. *Geochemistry Geophysics Geocystems* **6**, Q05007, doi:10.1029/2004GC000824.
Sturm M. E., Klein E. M., Graham D. W. & Karsten J. 1999. Age constraints on crustal recycling to the mantle beneath the southern Chile Ridge : He-Pb-Sr-Nd isotope systematics. *Journal of Geophysical Research* **104**, 5097–114.
Sun S.-S. & McDonough W. F. 1989. Chemical and isotopic systematic of oceanic basalts: Implications for mantle composition and processes. *In* Saunders A. D. and Norry M. J. (eds.) *Magmatism in the Ocean Basins*. Geological Society of London, Special Publications 42, pp. 313–45.
Tang Y.-J., Zhang H.-F. & Ying J.-F. 2006. Asthenosphere-lithospheric mantle interaction in an extensional regime: Implication from the geochemistry of Cenozoic basalts from Taihang mountains, North China Craton. *Chemical Geology* **233**, 309–27.
Taylor S. R. & McLennan S. M. 1985. *The Continental Crust: Its Composition and Evolution*. Blackwell, Oxford.
Tebbens S. F. & Cande S. C. 1997. Southeast Pacific tectonic evolution from early Oligocene to Present. *Journal of Geophysical Research* **102**, 12061–84.
Tebbens S. F., Cande S. C., Kovacs L., Parra J. C., LaBrecque J. L. & Vergara H. 1997. The Chile ridge: A tectonic framework. *Journal of Geophysical Research* **102**, 12035–60.
Thirlwall M. F. 1997. Pb isotopic and elemental evidence for OIB derivation from young HIMU mantle. *Chemical Geology* **139**, 51–74.
Thorkelson D. J. & Taylor R. P. 1989. Cordilleran slab windows. *Geology* **17**, 833–6.
Timm C., Hoernle K., Bogaard P. V. D., Bindemann I. & Weaver S. D. 2009. Geochemical evolution of intraplate volcanism at Banks Peninsula, New Zealand: interaction between asthenospheric and lithospheric melts. *Journal of Petrology* **50**, 989–1023.
Timm C., Hoernle K., Werner R. *et al*. 2010. Temporal and geochemical evolution of the Cenozoic intraplate volcanism of Zealandia. *Earth-Science Reviews* **98**, 38–64.
Todt W., Cliff R. A., Hanser A. & Hofmann A. W. 1996. Evaluation of a ^{202}Pb-^{205}Pb double spike for high precision lead isotope analyses. *In* Basu A. and Hart S. (eds.) *Earth Processes: Reading the Isotopic Code*, *Geophysical Monograph* 95, pp. 429–37, AGU, Washington DC.
Valera J. L., Negredo A. M. & Villaseñor A. 2008. Asymmetric delamination and convective removal numerical modeling: Comparison with evolutionary models for the Alboran sea region. *Pure and Applied Geophysics* **165**, 1683–706.
Wang J., Hattori K. H., Li J. & Stern C. R. 2008. Oxidation state of Paleozoic subcontinental lithospheric mantle below the Pali Aike volcanic field in southernmost Patagonia. *Lithos* **105**, 98–110.
Weaver B. L. 1991. The origin of ocean island basalt and end-member compositions: Trace element and isotopic constraints. *Earth and Planetary Science Letters* **104**, 381–97.
Weaver S. D., Storey B. C., Pankhurst R. J., Mukasa S. B., DiVenere V. J. & Bradshaw J. D. 1994. Antarctica-New Zealand rifting and Marie Byrd Land lithospheric magmatism linked to ridge subduction and mantle plume activity. *Geology* **22**, 811–4.
White W. M. 1985. Sources of oceanic basalts: Radiogenic isotopic evidence. *Geology* **13**, 115–8.
Willbold M. & Stracke A. 2006. Trace element composition of mantle end-members: Implications for recycling of oceanic and upper and lower continental crust. *Geochemistry Geophysics Geosystems* **7**, Q04004, doi:10.1029/2005GC001005.
Witt-Eickschen G. & Kramm U. 1998. Evidence for the multiple stage evolution of the subcontinental lithospheric mantle beneath the Eifel (Germany) from pyroxenite and composite pyroxenite/peridotite xenoliths. *Contributions to Mineralogy and Petrology* **131**, 258–72.
Workman R. K., Hart S. R., Jackson M. *et al*. 2004. Recycled metasomatized lithosphere as the origin of the Enriched Mantle II (EM2) end-member: Evidence from the Samoan Volcanic Chain. *Geochemistry Geophysics Geosystems* **5**, Q04008, doi:10.1029/2003GC000623.
Zindler A. & Hart S. R. 1986. Chemical geodynamics. Annual review. *Earth and Planetary Science Letters* **14**, 493–571.